

Atomically precise ultrasmall copper cluster for room-temperature highly regioselective dehydrogenative coupling

Received: 10 July 2023

Accepted: 18 October 2023

Published online: 28 October 2023

Check for updates

Teng Jia¹, Yi-Xin Li¹, Xiao-Hong Ma¹, Miao-Miao Zhang¹, Xi-Yan Dong ^{1,2}, Jie Ai¹ & Shuang-Quan Zang ¹✉

Three-component dehydrogenative coupling reactions represent important and practical methodologies for forging new C–N bonds and C–C bonds. Achieving highly all-in-one dehydrogenative coupling functionalization by a single catalytic system remains a great challenge. Herein, we develop a rigid-flexible-coupled copper cluster $[\text{Cu}_3(\text{NHC})_3(\text{PF}_6)_3]$ ($\text{Cu}_3\text{NC}^{(\text{NHC})}$) using a tridentate N-heterocyclic carbene ligand. The shell ligand endows $\text{Cu}_3\text{NC}^{(\text{NHC})}$ with dual attributes, including rigidity and flexibility, to improve activity and stability. The $\text{Cu}_3\text{NC}^{(\text{NHC})}$ is applied to catalyze both highly all-in-one dehydrogenative coupling transformations. Mechanistic studies and density functional theory illustrate that the improved regioselectivity is derived from the low energy of ion pair with copper acetylide and *endo*-iminium ions and the low transition state, which originates from the unique physicochemical properties of the $\text{Cu}_3\text{NC}^{(\text{NHC})}$ catalyst. This work highlights the importance of N-heterocyclic carbene in the modification of copper clusters, providing a new design rule to protect cluster catalytic centers and enhance catalysis.

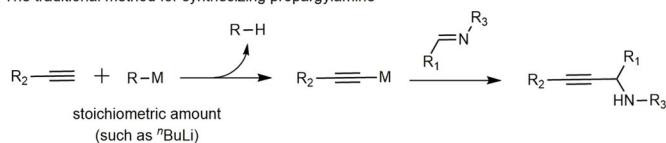
Propargylamines including C1-propargylamines are essential building blocks for organic synthesis, the production of pharmaceuticals and compounds of substantial synthetic value industry^{1–3}, including oxazolidines⁴, cavidine⁵, 6-amino-pyridones⁶, solifenacin⁷, apomorphine⁸, naspamine⁹ and so on. Thus, much investigation has been devoted to the synthesis of propargylamine and C1-propargylamine compounds. For synthesizing propargylamines (Fig. 1a, b), researchers commonly exploit the different ways to form metal acetylides, such as the terminal acetylenes activation of bases or transition-metal salts, then the addition of the metal acetylides to imines to synthesize propargylamines^{10–19}. For synthesizing C1-propargylamines (Fig. 1c), the copper compounds as representative catalysts could catalyze the redox-A³ coupling reaction under specific conditions³. The α -amino acid^{20–22}, simple amine^{23–25} and tertiary amine^{26,27} as representative amine reactants were used in the organic transformations under the hard conditions by Li²⁰, Seidel^{21,23}, and Ma²⁵

et al. Due to the unique physicochemical properties of copper, earth-abundant and inexpensive, the copper compounds are one of the most representative catalysts in both organic transformations. However, challenges of existing catalytic systems still remain, especially copper catalytic systems: Lack of the catalytic system that could catalyze efficiently and regioselectively both the A³ coupling reaction and the redox-A³ reaction with broad substrates scope of aliphatic aldehydes, alkynes and amines under mild conditions. Efficient and practical new copper-basic material catalysts to achieve both reactions at room temperature are highly desirable.

Metal nanoclusters (NCs) are highly representative nanostructured material catalysts that are widely used in various catalytic transformations, such as chemical preparation, energy catalysis and electrochemical catalysis^{28–31}. In contrast to metal nanoparticles (NPs), ligand-protected NCs with well-defined structures, high surface-to-volume ratios, and molecular purity can provide active sites with

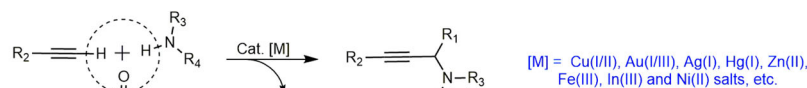
¹Henan Key Laboratory of Crystalline Molecular Functional Materials, Henan International Joint Laboratory of Tumor Theranostical Cluster Materials, Green Catalysis Center, and College of Chemistry, Zhengzhou University, Zhengzhou, P. R. China. ²College of Chemistry and Chemical Engineering, Henan Polytechnic University, Jiaozuo, P. R. China. ✉ e-mail: zangsqzq@zzu.edu.cn

(a) The traditional method for synthesizing propargylamine



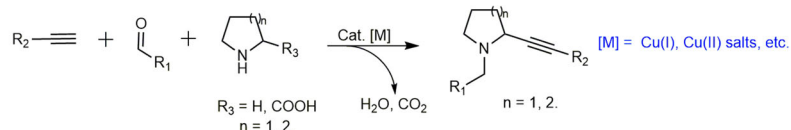
- Required stoichiometric amount of strong bases and the high moisture sensitivity

(b) The transition-metal catalyzed the A³ coupling reaction



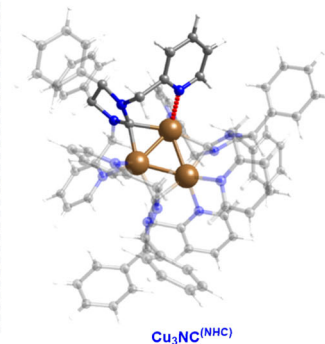
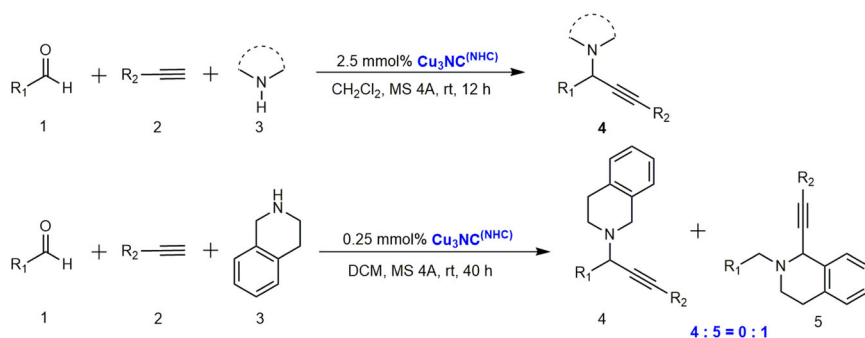
-The aliphatic aldehydes, alkynes and amines usually react worst than aromatic under mild condition

(c) The transition-metal catalyzed the redox-A³ coupling reaction



-Required hard condition (such as microwave, high temperature, etc.)

(d) **This work:** The Cu₃NC^(NHC) catalyzed both the A³ coupling reaction and the redox-A³ coupling reaction



- N-heterocyclic carbene-stabilized Cu₃ nanoclusters

- 71 examples of A³ coupling, up to 99% yield

- C-C, C-N coupling at room temperature

- Highly catalytically active and highly regioselective

- 14 examples of redox-A³ coupling, up to 99% yield, 4 : 5 = 0 : 1

- Both aliphatic and aromatic aldehydes, alkynes, cyclic and acyclic aliphatic amines

Fig. 1 | Representative synthesis strategies of propargylamines and C1-propargylamines. **a** The traditional method for synthesizing propargylamine. **b** The transition-metal catalyzed the A³ coupling reaction. **c** The transition-metal

catalyzed the redox-A³ coupling reaction. **d** This work: The Cu₃NC^(NHC) catalyzed both the A³ coupling reaction and the redox-A³ coupling reaction. R₁, R₂, R₃ and R represent kinds of functional group.

relatively uniform distributions, facilitate activation of reactants, allow techniques for activity and selectivity control in certain cases, and reveal the correlation between the structure and catalytic performance at the atomic scale^{32–34}. Importantly, unlike organometallic catalysts, NCs catalysts with metal-metal interactions are conducive to achieving the synergistic catalysis effect of multiple metals in the special organic transformations, potentially improving practical properties of the catalysts^{32–35}. However, the exploration of copper NCs is more uncommon than that of other coin metal NCs. The long-term stability of copper NCs in organic transformation systems may remain an unrealized problem. The versatile ligands of N-heterocyclic carbenes (NHCs) are widely used in diverse transition metal catalysts for catalytic organic transformations^{36–39}. Due to the high modularity of NHC structures, the unique steric and electronic effects and formation of stable C–metal bonds between the NHC ligands and metal atom, NHC ligands are ideal candidates for improving the stability and reactivity of copper NC catalysts through ligand engineering effects^{39–41}. Copper NCs have not been investigated as the model catalysts to realize highly all-in-one dehydrogenative coupling reactions at room temperature.

Herein, we design and develop a tridentate N-heterocyclic carbene that serves as the protected ligand of copper NCs, and a rigid-

flexible-coupled copper cluster [Cu₃(NHC)₃(PF₆)₃] (Cu₃NC^(NHC)) is constructed successfully in the gram scale. The designed N-heterocyclic carbene ligand endows Cu₃NC^(NHC) with dual attributes of rigidity and flexibility. Due to the formation of the stable C–Cu bonds and the N–Cu coordination bonds between the NHC ligand shell with the dynamic L-ligand (DLL, L: NHC) and the metal core, this ligand can improve the Cu₃NC^(NHC) rigidity, which is beneficial for further enhancing the stability of the Cu₃NC^(NHC). The pyridine of the N-heterocyclic carbene is designed as DLL, which favors a dynamic balance between the pyridine and aliphatic amines to protect catalytic centers and prevent Cu₃NC^(NHC) deactivation. The dissociation and coordination of DLL endow Cu₃NC^(NHC) with flexible features, further improving regioselective dehydrogenative coupling reactions through weak interactions between dissociated pyridines and reactants. Importantly, the Cu₃NC^(NHC) catalyst is applied to achieve efficient and regioselective all-in-one three-component dehydrogenative coupling reactions with inert substrates at room temperature (Fig. 1d). By combining single-crystal structure analyses, experimental characterizations, and DFT calculations, we find the highly regioselective dehydrogenative coupling mechanisms and the relationships between structures and catalytic performance characteristics.

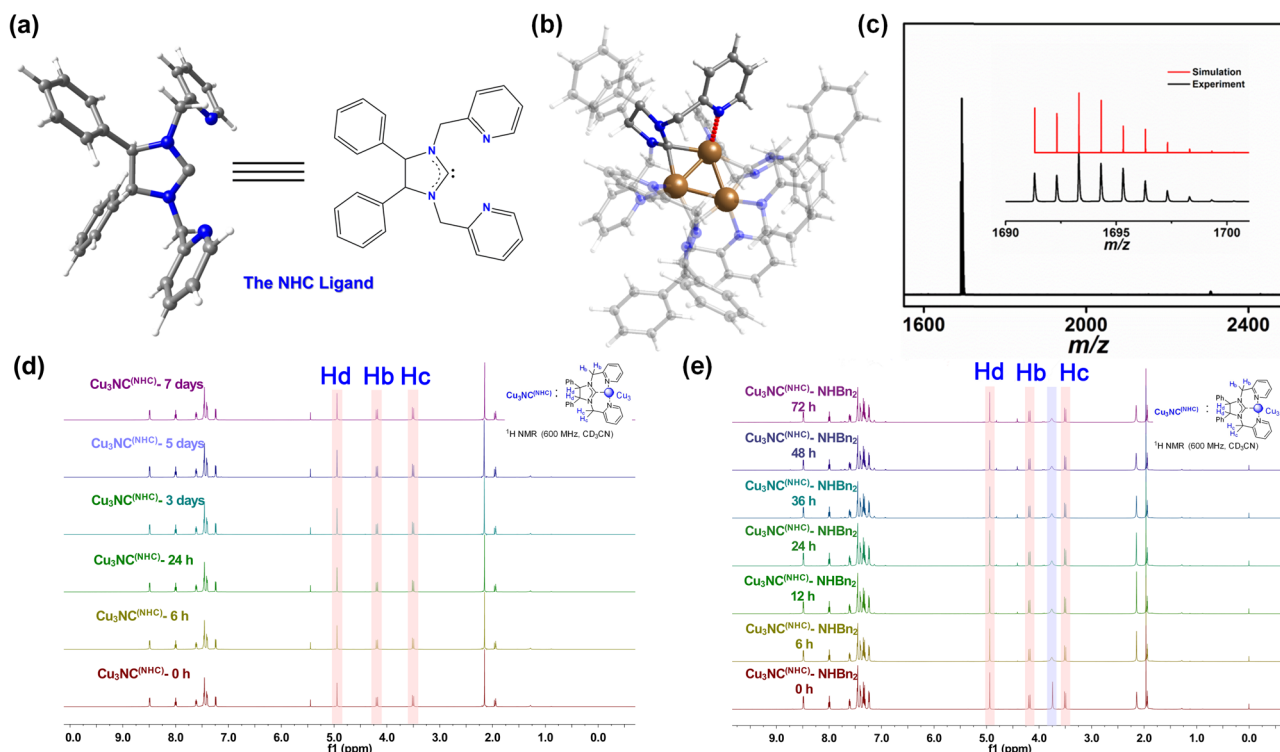


Fig. 2 | Schematic illustration and characterization of $\text{Cu}_3\text{NC}(\text{NHC})$. **a** Structure of the N-heterocyclic carbene (NHC) ligand. Color legend: blue, N; gray, C; and white, H. **b** Total structure of the $\text{Cu}_3\text{NC}(\text{NHC})$. Color legend: brown, Cu; blue, N; gray, C; and white, H. **c** ESI-MS spectra of $\text{Cu}_3\text{NC}(\text{NHC})$ dissolved in dimethylformamide (DMF)/DCM solution and measured in the positive mode. Inset: experimental (black) and

simulated (red) isotopic distributions of $\text{Cu}_3\text{NC}(\text{NHC})$. **d** ^1H NMR spectra of $\text{Cu}_3\text{NC}(\text{NHC})$ in MeCN-d_3 (0–7 days). Hd, Hb and Hc represent the characteristic H atoms of $\text{Cu}_3\text{NC}(\text{NHC})$. **e** ^1H NMR spectra of $\text{Cu}_3\text{NC}(\text{NHC})\cdot\text{HNBn}_2$ (1:3) in MeCN-d_3 (0–72 h). Hd, Hb and Hc represent the characteristic H atoms of the $\text{Cu}_3\text{NC}(\text{NHC})$. The characteristic peaks in the pale blue box represent the methylene peak of the HNBn_2 .

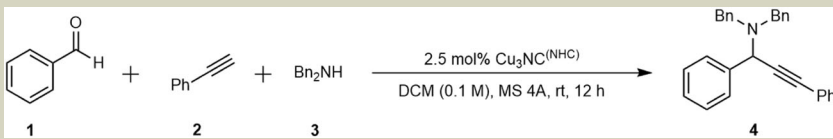
Results

Catalyst development and characterization

The N-heterocyclic imidazolium salt 4,5-diphenyl-1,3-bis(pyridin-2-ylmethyl)-4,5-dihydro-1H-imidazol-3-ium chloride was designed and synthesized by the condensation reaction and the nucleophilic substitution transformation (Supplementary Fig. 1), forming a model tridentate NHC ligand including a 5-membered N-heterocyclic carbene and two pyridines of DLL in NCs (Fig. 2a). $\text{Cu}_3\text{NC}(\text{NHC})$ was prepared using the designed tridentate NHC ligand and copper powder as the copper source. The $[\text{Cu}_3(\text{BINAP})_3\text{CO}_3](\text{tBuSO}_3)$ ($\text{Cu}_3\text{NC}(\text{BINAP})$) and the $\text{Cu}_3(3,5\text{-Ph}_2\text{-Pz})_3$ ($\text{Cu}_3\text{NC}(\text{Pz})$) were synthesized by employing 2,2-bis(diphenylphosphino)-1,1'-binaphthyl (BINAP) and 3,5-diphenylpyrazole (Pz) ligands, respectively, through solvent diffusion methods^{42,43}. More synthetic details can be found in the Supplementary Information. Single-crystal X-ray analysis revealed that $\text{Cu}_3\text{NC}(\text{NHC})$ contained a triangle Cu_3 metal kernel that was stabilized by three NHC ligands, in which three PF_6^- anions balanced the charges (Fig. 2b). Due to the perpendicular orientation of the carbene ligands to the Cu_3 face in $\text{Cu}_3\text{NC}(\text{NHC})$, the pyridine rings of the NHC ligands could alternate their coordination above and below the Cu_3 plane. Of the three NHC ligands, all ligands bonded to the Cu_3 core in the same coordination manner via Cu–C bonds and Cu–N bonds, which improved the $\text{Cu}_3\text{NC}(\text{NHC})$ rigidity and the stability of $\text{Cu}_3\text{NC}(\text{NHC})$. The flexibility of $\text{Cu}_3\text{NC}(\text{NHC})$ originates in the flexible bonding and dissociation between pyridine groups of ligands and Cu centers. When the original pyridine moieties in DLL ligands were dissociated from Cu_3 core in the catalytic systems, pyridines could rotate freely to decrease the steric hindrance around the copper center, making the catalytic center exposed to the catalytic substrate. While the reaction was completed, pyridine groups reversibly coordinated to Cu atoms, restoring the original structure of the cluster. The flexibility ensures the stability and reversibility of this copper cluster catalyst. The Cu–Cu distances of $\text{Cu}_3\text{NC}(\text{NHC})$ ranged

from 2.4960 to 2.5238 Å with an average distance of 2.5124 Å; this value is shorter than the sum of the van der Waals radii of copper (2.8 Å), suggesting the presence of strong metal-metal interactions^{44,45}. To ascertain the exact molecular masses and formulas of the clusters, $\text{Cu}_3\text{NC}(\text{NHC})$ and $\text{Cu}_3\text{NC}(\text{BINAP})$ were further characterized by electrospray ionization mass spectrometry (ESI-MS) in positive mode (Fig. 2c, Supplementary Figs. 7 and 8). For $\text{Cu}_3\text{NC}(\text{NHC})$, the spectrum depicted prominent peaks at m/z 1693.316, corresponding to the molecular ion of $[\text{Cu}_3(\text{NHC})_3(\text{PF}_6)_2]^+$ (calcd m/z 1693.315) (Fig. 2c). For $\text{Cu}_3\text{NC}(\text{BINAP})$, the peak with high abundance at m/z 2118.375 was assigned to $[\text{Cu}_3(\text{BINAP})_3\text{CO}_3]^+$ (calcd m/z 2118.375) (Supplementary Fig. 8). The molecular ion peaks of $\text{Cu}_3\text{NC}(\text{NHC})$ and $\text{Cu}_3\text{NC}(\text{BINAP})$ were in precise agreement between experimental and simulated isotopic distributions.

The phase purities of $\text{Cu}_3\text{NC}(\text{NHC})$, $\text{Cu}_3\text{NC}(\text{BINAP})$ and $\text{Cu}_3\text{NC}(\text{Pz})$ were confirmed by powder X-ray diffraction measurements (Supplementary Figs. 4–6). In addition, the nuclear magnetic resonance (NMR) spectra of these clusters were characterized (Supplementary Figs. 9–14). According to the in situ ^1H NMR spectra of $\text{Cu}_3\text{NC}(\text{NHC})$ in CD_3CN or basic solvent, the characteristic peaks of $\text{Cu}_3\text{NC}(\text{NHC})$ were not shifted for 7 days or 72 h, confirming that $\text{Cu}_3\text{NC}(\text{NHC})$ is very stable in organic solvents (Fig. 2d, e). Supplementary Fig. 15 displayed the ultraviolet–visible (UV–vis) absorption spectrum of $\text{Cu}_3\text{NC}(\text{NHC})$ in dichloromethane (DCM), with three characteristic peaks at 290 nm, 346 nm and 389 nm. In addition, time-dependent UV–vis spectra showed no discernible change in DCM or basic solvent (Supplementary Figs. 16 and 17). The UV–vis absorption behavior of $\text{Cu}_3\text{NC}(\text{BINAP})$ in DCM or basic solvent was unchanged after 72 h of treatment (Supplementary Figs. 18 and 19). The time-dependent UV–vis spectra of $\text{Cu}_3\text{NC}(\text{Pz})$ showed no change in DCM (Supplementary Fig. 20). The in situ ^1H NMR spectra of the $\text{Cu}_3\text{NC}(\text{Pz})$ characteristic peaks in CD_3Cl or basic solvent were not shifted after 148 h and 72 h of treatment,

Table 1 | Optimization of A³ coupling reaction conditions^{a,b}


Entry	Variations	Conv.	Yield of 4
1	None	100%	99%
2	2 h	65%	65%
3	5 h	100%	99%
4	Cu ₃ NC ^(BINAP) , 5 h	70%	68%
5	Cu ₃ NC ^(Pz) , 5 h	27%	25%
6	5 mol% CuBr, 5 h	50%	48%
7	5 mol% CuCl, 5 h	28%	27%
8	5 mol% Cu ₂ O, 5 h	trace	trace
9	Cu(MeCN) ₄ PF ₆ , 5 h	61%	59%
10	Dioxane as solvent	20%	<10%
11	THF as solvent	30%	15%
12	MeOH as solvent	n.r.	n.r.
13	MeCN as solvent	70%	53%
14	No copper	n.r.	n.r.
15	NHC ligand	n.r.	n.r.
16	No 4 Å MS	20%	20%

^aGeneral reaction conditions: 1 (0.2 mmol, 1.0 equiv.), 2 (0.2 mmol, 1.0 equiv.), 3 (0.3 mmol, 1.5 equiv.), [Cu] catal. (0.005 mmol, 2.5 mol%), activated MS 4 Å sieves (600 mg) in dry solvent (2.0 mL) under N₂ at room temperature.

^bConversion and yield were determined by ¹H NMR using 1,3,5-trimethoxybenzene as an internal standard.

respectively (Supplementary Figs. 24 and 25). All the characterization of the clusters indicated that Cu₃NC^(NHC), Cu₃NC^(BINAP) and Cu₃NC^(Pz) were successfully synthesized, and their structures were retained intact in organic solvents.

A³ coupling and redox-A³ coupling reaction development

By investigating the structural and chemical characteristics of Cu₃NC^(NHC), we tested the material performance in both organic transformations. Initially, by using 2.5 mol% Cu₃NC^(NHC) as the catalyst, benzaldehyde 1 (0.2 mmol, 1.0 eq.), phenylacetylene 2 (0.2 mmol, 1.0 eq.), molecular sieves (MS) 4 Å sieves, dibenzylamine 3 (0.3 mmol, 1.5 eq.) and dry DCM (2 mL) were added to dry Schlenk tube in proper order and stirred under N₂ atmosphere at room temperature for 2 h to examine the catalytic activity of Cu₃NC^(NHC) in the A³ coupling reaction (Table 1, entry 2). Surprisingly, Cu₃NC^(NHC), as a new type catalyst, catalyzed the A³ coupling reaction, affording the desired typical propargylamine product with good yields (65%). Previously, it was reported that Au NPs and metal nanoclusters were utilized as catalysts to catalyze the A³ coupling reaction under harsh conditions by Vinu and Jin's group et al.^{46–54}. Strikingly, the Cu₃NC^(NHC) catalyst could efficiently catalyze the A³ coupling reaction at room temperature. Inspired by this result, we set the goal to explore the possibility of the Cu₃NC^(NHC) as a catalyst, which was employed in the A³ coupling reaction. The performance attributes of some alternative conditions are summarized in Table 1.

As shown in Table 1, an excellent yield (99%) of the desired propargylamine product was obtained by prolonging the reaction time from 2 to 5 h (Table 1, entries 2 and 3). Under the same reaction conditions, Cu₃NC^(BINAP) and Cu₃NC^(Pz) as catalysts could catalyze the A³ coupling reaction, providing propargylamine in good yields (68%) and poor yields (25%) at room temperature for 5 h, respectively (Table 1, entries 4 and 5). For the A³ coupling reaction, Cu₃NC^(NHC)

exhibited higher catalytic activities than Cu₃NC^(BINAP) and Cu₃NC^(Pz). Interestingly, propargylamine with excellent yield (99%) was still obtained (Table 1, entry 1) when Cu₃NC^(NHC) was utilized as the catalyst in the A³ coupling reaction and the reaction time was prolonged from 5 to 12 h. The results showed that Cu₃NC^(NHC) was a mild catalyst for propargylamine at room temperature. Notably, the load of the Cu₃NC^(NHC) catalyst could be reduced to 0.025 mol% such that the A³ coupling transformation reacted in a higher turnover number (TON) of 3800 than other catalysts at room temperature (Supplementary Table 1)^{46,55,56}.

As observed, the 5 mol% CuBr, 5 mol% CuCl, 5 mol% Cu₂O and Cu(MeCN)₄PF₆ catalysts only had poor to modest yields after 5 h (48%, 27%, trace and 59%, respectively; Table 1, entries 6–9). The other solvents (dioxane, tetrahydrofuran (THF), MeCN and MeOH) were not suitable with a seriously decreased yield (Table 1, entries 10–13). The control experiments showed that activated MS 4 Å sieves alone or the NHC ligand as a catalyst could not catalyze the reaction (Table 1, entries 14 and 15). In addition, the lack of activated MS 4 Å sieves was not conducive to obtaining a great yield of the desired propargylamine product (Table 1, entry 16). In the three-component dehydrogenative coupling reaction systems, the activated MS 4 Å sieves, as a kind of adsorption drying agent, could remove by-product water in time, enhancing dehydrogenative coupling reactions rate and improving the yields of propargylamines to 99%. Moreover, Cu₃NC^(NHC) remained intact in the organic catalytic system when serving as the catalyst, as practically no apparent changes in the UV–vis spectra, the in situ ¹H NMR and ESI–MS monitoring of organic reaction process were found before and after the transformation (Supplementary Figs. 26–28). These results indicated that multiple C–Cu bonds and N–Cu coordination bonds between the NHC ligands and Cu₃ core could enhance the stability of the Cu₃NC^(NHC) by way of improving the rigidity of Cu₃NC^(NHC).

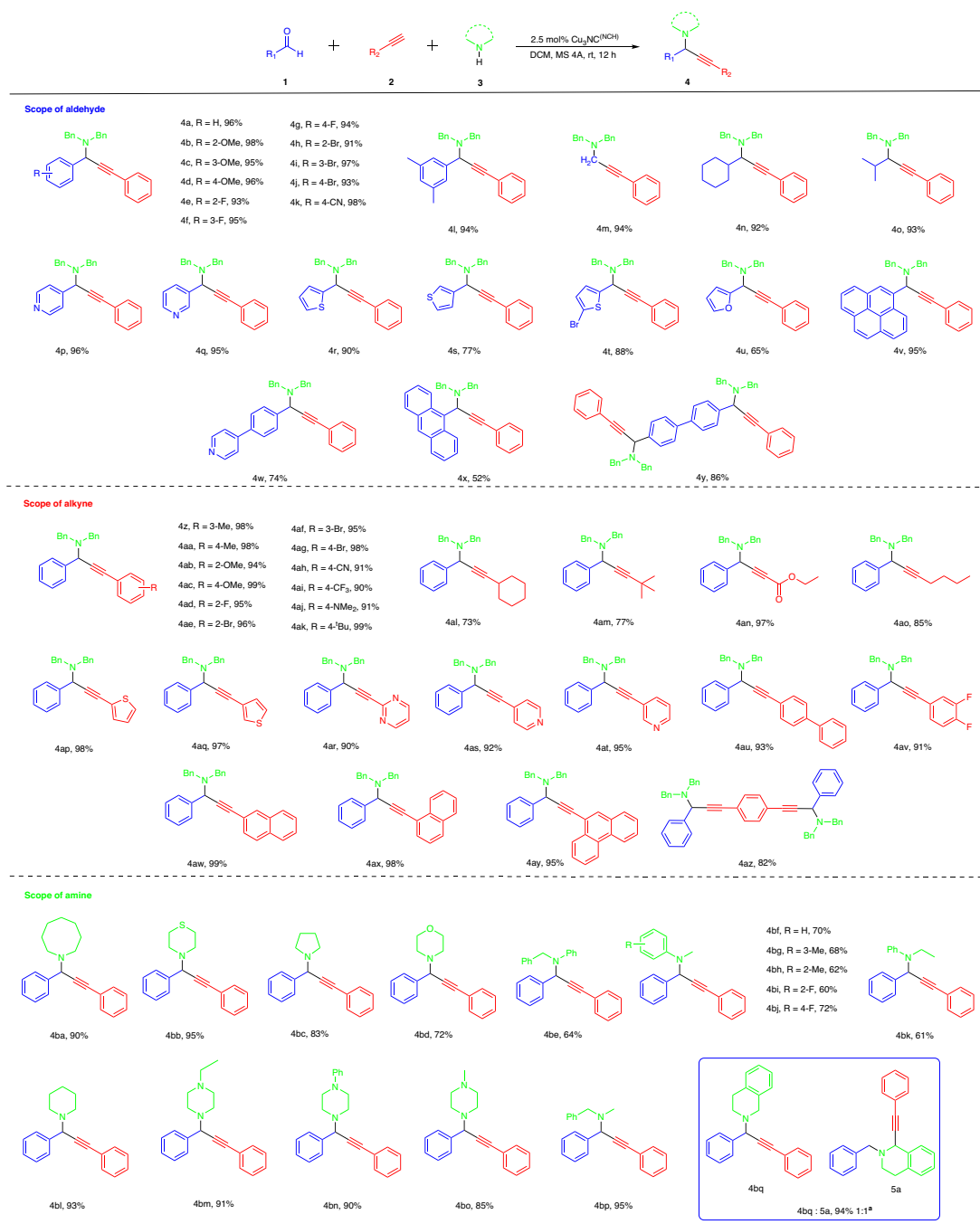


Fig. 3 | The A^3 coupling reaction scope for aldehydes, alkynes and amines. General reaction conditions: 1 (0.2 mmol, 1.0 equiv.), 2 (0.2 mmol, 1.0 equiv.), 3 (0.3 mmol, 1.5 equiv.), $Cu_3NC^{(NHC)}$ (0.005 mmol, 2.5 mol%), activated MS 4 Å sieves

(600 mg) in dry solvent (2.0 mL) under N_2 at room temperature. Isolated yields are given. *The ratio of **4bp** and **5a** was determined by crude 1H NMR spectra of the reaction mixture.

Under the optimal conditions, the substrate scopes of the A^3 coupling reaction, including aldehydes, alkynes, and amines, were evaluated. The results are summarized in Fig. 3. We first evaluated the scope of aldehydes. Various aldehydes were prepared as coupling companions with alkynes and amines. For aryl aldehydes (**4a–4l**), the reaction was applicable to both electro-deficient and electron-rich aromatic rings, providing the desired propargylamine products in excellent yields. Aliphatic aldehydes afforded the desired A^3 coupling products with excellent yields (**4m–4o**). Notably, electron-deficient heterocyclic pyridine aldehydes, the electron-rich heterocyclic thiophene aldehydes and furan aldehydes were suitable substrates for this transformation with good to excellent yields (**4p–4u**). In addition to

the abovementioned aldehydes, aryl aldehydes containing large substituent groups were explored; these aryl aldehydes performed well, providing the desired products in modest to excellent yields (**4v–4x**). Meanwhile, aryl dialdehyde was a very suitable substrate for this reaction with excellent yield (**4y**).

Various alkynes, including aliphatic and aryl alkynes, were applied to this transformation. Similar to aldehyde substrates, $Cu_3NC^{(NHC)}$ as the catalyst was widely applicable to various alkynes. Both aryl alkynes (**4z–4ak**, **4av**) and aliphatic alkynes (**4al–4ao**), including electro-deficient and electron-rich functional groups, displayed good to excellent yields. Both S-heterocyclic and N-heterocyclic aryl alkynes were suitable substrates for this transformation and afforded excellent

yields (**4ap–4at**). Furthermore, aryl alkynes containing large substituent groups and aryl dialkyne were investigated and these aryl alkynes worked well, affording the corresponding products in excellent yields (**4au, 4aw–4az**) and further supporting our hypothesis of $\text{Cu}_3\text{NC}^{\text{(NHC)}}$ with the flexible feature that the dissociation of Cu–N bonds between pyridine groups and Cu_3 core allowed pyridines to rotate freely through the C–C single bond, thereby decreasing the steric hindrance around copper catalytic center and enhanced the catalytic activity.

In addition, a series of amines were explored in the reaction. To our satisfaction, the N-heterocyclic secondary amines were applicable to this transformation with great to excellent yields at room temperature (**4ba, 4bc and 4bi**). Both piperazines with different substituent groups and morpholines (including thiomorpholine) displayed high reactivities and afforded good to excellent yields (**4bb, 4bd, 4bm–4bo**). These results highlighted that the pyridine of the DLL was crucial for the $\text{Cu}_3\text{NC}^{\text{(NHC)}}$ catalyst to present a dynamic balance between the DLL and aliphatic amines, maintaining the efficient catalytic activity. Undoubtedly, acyclic secondary amines with the electron-deficient and electron-rich fundamental groups readily afforded propargylamines in good to excellent yields (**4be–4bk, 4bp**). The primary amines, aniline, p-toluidine, 4-fluoroaniline, amantadine, thiophene-2-ethylamine, and 1-octylamine, did not offer propargylamine products, which are considered to be inert substrates for A^3 -coupling transformations under mild conditions^{57,58}. Interestingly, when 1,2,3,4-tetrahydroisoquinoline (THIQs) was used to this transformation, the products of propargylamine and CI-propargylamine were obtained in excellent yields and modest regioselectivity (**4bq and 5a**). Strikingly, the ratio of product **4bq** to product **5a** was 1:1, as determined by ^1H NMR. This finding demonstrated that the unique physicochemical properties of the designed $\text{Cu}_3\text{NC}^{\text{(NHC)}}$ catalyst, including the weak interactions between dissociated DLL and reactants, led to this result.

To our knowledge, no one catalytic system could catalyze both the A^3 coupling reaction and the redox- A^3 reaction at room temperature in an efficient and regioselective manner to date. By considering the catalytic diversity of $\text{Cu}_3\text{NC}^{\text{(NHC)}}$, the $\text{Cu}_3\text{NC}^{\text{(NHC)}}$ was investigated as a new typical catalyst for the synthesis of the desired CI-propargylamine products. As seen in Table 2, with decreasing catalyst loading of $\text{Cu}_3\text{NC}^{\text{(NHC)}}$ from 2.5 to 0.25 mol% and increasing reaction time from 12 to 40 h, the yields of the CI-propargylamine product increased from 48% to 98%, and the regioselectivity gradually increased to 100% at room temperature (Table 2, entries 1–5). By employing toluene as the solvent, the reaction afforded 100% regioselectivity, but the yield was poor (Table 2, entries 6 and 7). To improve the yields of CI-propargylamine, a mixed solvents of toluene-DCM was used in the catalytic system with a slightly improved yield, but the regioselectivity was seriously decreased (Table 2, entries 8 and 9). Notably, the load of the $\text{Cu}_3\text{NC}^{\text{(NHC)}}$ catalyst could be lowered to 0.025 mol% such that the redox- A^3 coupling transformation reacted in a high TON of 1840 (Supplementary Table 2). For comparison, the $\text{Cu}_3\text{NC}^{\text{(BINAP)}}$, $\text{Cu}_3\text{NC}^{\text{(Pz)}}$ and copper salts as catalysts were investigated. Under the optimal reaction conditions, $\text{Cu}_3\text{NC}^{\text{(BINAP)}}$ and $\text{Cu}_3\text{NC}^{\text{(Pz)}}$ as catalysts could catalyze the redox- A^3 coupling reaction giving CI-propargylamines with moderate to poor yields (50%, 25%) and poor to great the regioselectivity (**4bp:5a**, 1:5 and 0:1) at room temperature (Table 2, entries 10 and 11). As observed, the CuI and $\text{Cu}(\text{MeCN})_4\text{PF}_6$ catalysts, which were 5 times the catalyst loading of the $\text{Cu}_3\text{NC}^{\text{(NHC)}}$, had modest yields and poor regioselectivity (Table 2, entries 12 and 13). The control experiment showed that neither activated MS 4 Å sieves nor the NHC ligand as a catalyst could catalyze the reaction (Table 2, entries 14 and 15). In addition, the $\text{Cu}_3\text{NC}^{\text{(NHC)}}$ catalyst showed excellent stability in the organic catalytic system, as demonstrated by ESI-MS spectra monitoring before and after the transformation (Supplementary Fig. 29).

Under the optimized conditions, the substrate scope of the redox- A^3 coupling reaction, including aldehydes and alkynes, was evaluated (Fig. 4). First, the scope of aldehydes was evaluated. A range of aldehydes were prepared as coupling companions with alkynes and THIQs. For aryl aldehydes (**5a–5d**), the reaction performed well for both electro-deficient and electron-rich aromatic rings, offering the desired CI-propargylamine products in high yields and good to excellent regioselectivity. Furthermore, the electron-rich heterocyclic thiophene aldehydes, aryl aldehydes containing large substituent groups and aliphatic aldehyde afforded the desired and single redox- A^3 coupling product with excellent yields (**5e–5g**). Next, various alkynes were explored. Both aryl alkynes (**5h–5k**) and aliphatic alkynes (**5n**) with electro-deficient and electron-rich functional groups were well applied to the reaction in high yields and excellent regioselectivity. Interestingly, both aryl alkynes containing large substituent groups and S-heterocyclic aryl alkynes were tolerated in the $\text{Cu}_3\text{NC}^{\text{(NHC)}}$ -catalyzed redox- A^3 coupling reaction, giving single and excellent yields of CI-propargylamines (**5l and 5m**). Finally, the other secondary amines, N-phenylbenzylamine (**3be**), 1-ethylpiperazine (**3bm**), 1-phenylpiperazine (**3bn**), N-methylbenzylamine (**3bp**), and pyrrolidine (**3bc**), were utilized to the redox- A^3 coupling transformation under optimized conditions. Regrettably, the redox- A^3 coupling products were not observed, indicating that in situ-generated exo-iminium ions are not always easy to isomerize to *endo*-iminium ions.

Mechanistic studies and density functional theory (DFT) calculations

To clarify why $\text{Cu}_3\text{NC}^{\text{(NHC)}}$ could catalyze highly all-in-one three-component dehydrogenative coupling reactions and to gain insight into the catalytic mechanism of these transformations, DFT calculations and a series of control experiments were conducted. First, the characteristic peaks of the benzyl-methylene proton of NHBn_2 began to broaden in the in situ ^1H NMR spectra of the mixture the $\text{Cu}_3\text{NC}^{\text{(NHC)}}$ and NHBn_2 with increasing reaction time, and the characteristic peaks of $\text{Cu}_3\text{NC}^{\text{(NHC)}}$ were slightly shifted (Fig. 2e, Supplementary Figs. 22 and 23). The results illustrated that $\text{Cu}_3\text{NC}^{\text{(NHC)}}$, which was coordinated with the N atom of NHBn_2 , had good adsorption ability on amine reactants. Moreover, we considered the bonding and adsorption characteristics of alkynyl substrates on the surface active site of $\text{Cu}_3\text{NC}^{\text{(NHC)}}$ by using 2-fluorophenylacetylene (2-F-PA) as an example, which was convenient for ^1H and ^{19}F NMR to follow the transformations process. Experimentally, obvious chemical shifts were revealed for the in situ ^1H and ^{19}F NMR spectra of the 2-F-PA after mixing with the $\text{Cu}_3\text{NC}^{\text{(NHC)}}$, and the characteristic peaks of the catalyst were slightly shifted in the in situ ^1H NMR and ^{19}F NMR spectra, demonstrating a non-negligible interaction between the acetylene of 2-F-PA and $\text{Cu}_3\text{NC}^{\text{(NHC)}}$ (Supplementary Figs. 31 and 32). Next, we explored the transformations process of the A^3 coupling reaction and redox- A^3 coupling reaction by taking the in situ ^{19}F NMR spectra, suggesting that the characteristic peaks of 2-F-PA started to gradually disappear at -110.10 ppm and the characteristic peaks of the propargylamines and CI-propargylamines began to appear at -109.42 ppm and -109.70 ppm, respectively (Supplementary Figs. 33 and 34), indicating the $\text{Cu}_3\text{NC}^{\text{(NHC)}}$ catalyst possessed the excellent regioselectivity in the A^3 coupling reaction and redox- A^3 coupling reaction. Finally, to obtain convincing evidence for the $\text{Cu}_3\text{NC}^{\text{(NHC)}}$ -activated deprotonation of alkynes to form $\text{R}_1\text{C}\equiv\text{CCu}_3\text{NC}$, the control experiments were designed to prove the mechanism of $\text{Cu}_3\text{NC}^{\text{(NHC)}}$ -activated deprotonation of alkynes, in which the $\text{PhC}\equiv\text{CD}$ instead of $\text{PhC}\equiv\text{CH}$ was used in the A^3 coupling reaction and redox- A^3 coupling reaction. The characteristic peaks of D were not present in the ^2H NMR spectra of the purified propargylamines and CI-propargylamines (Supplementary Fig. 35), revealing that the terminal D fell off and formed $\text{R}_1\text{C}\equiv\text{CCu}_3\text{NC}$ during the A^3 coupling reaction and redox- A^3 coupling reaction.

Table 2 | Optimization of redox-A³ coupling reaction conditions^{a,b}

Entry	Variations	Conv.	Yield of 4bp	Yield of 5a	Ratio
1	None	100%	—	98%	0:1
2	2.5 mol% Cu ₃ NC ^(NHC) , 12 h	100%	47%	47%	1:1
3	1.0 mol% Cu ₃ NC ^(NHC) , 12 h	82%	17%	63%	1:3.7
4	0.5 mol% Cu ₃ NC ^(NHC) , 20 h	78%	11%	66%	1:6
5	0.25 mol% Cu ₃ NC ^(NHC) , 32 h	82%	—	82%	0:1
6	2.5 mol% Cu ₃ NC ^(NHC) , Toluene, 12 h	16%	—	14%	0:1
7	2.5 mol% Cu ₃ NC ^(NHC) , Toluene, 50 °C, 6 h	34%	—	30%	0:1
8	2.5 mol% Cu ₃ NC ^(NHC) , Toluene-DCM 1:1, 12 h	38%	2%	35%	1:17.5
9	2.5 mol% Cu ₃ NC ^(NHC) , Toluene-DCM 1:4, 12 h	70%	20%	50%	2:5
10	0.25 mol% Cu ₃ NC ^(BIMP)	62%	10%	50%	1:5
11	0.25 mol% Cu ₃ NC ^(Pz)	27%	—	25%	0:1
12	1.25 mol% CuI	66%	10%	56%	1:5.6
13	1.25 mol% Cu(MeCN) ₄ PF ₆	30%	—	26%	0:1
14	No copper	n.r	n.r	n.r	—
15	NHC ligand	n.r	n.r	n.r	—

^aGeneral reaction conditions: 1 (0.2 mmol, 1.0 equiv.), 2 (0.2 mmol, 1.0 equiv.), 3 (0.3 mmol, 1.5 equiv.), [Cu] catal. (0.0005 mmol, 0.25 mol%), activated MS 4 Å sieves (600 mg) in dry solvent (2.0 mL) under N₂ at room temperature.

^bConversion, ratio of **4bp** and **5a**, yield of **4bp** and yield of **5a** were determined by ¹H NMR using 1,3,5-trimethoxybenzene as an internal standard.

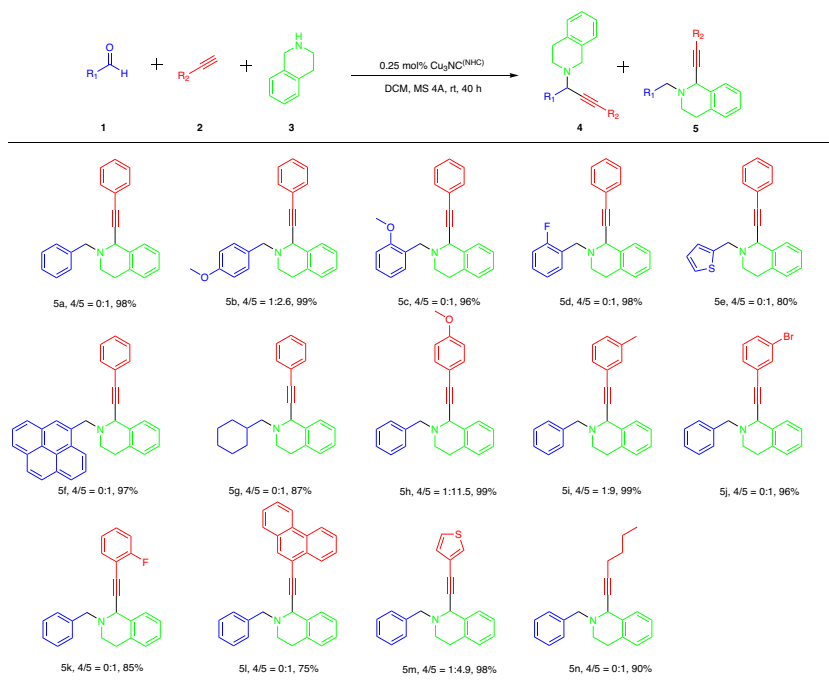


Fig. 4 | Redox-A³ coupling reaction scope for aldehydes and alkynes. General reaction conditions: 1 (0.2 mmol, 1.0 equiv.), tetrahydroisoquinoline 2 (0.2 mmol, 1.0 equiv.), 3 (0.3 mmol, 1.5 equiv.), Cu₃NC^(NHC) (0.0005 mmol, 0.25 mol%), activated

MS 4 Å (600 mg) in dry solvent (2.0 mL) under N₂ at room temperature. Isolated yields are given. The ratio of 4 and 5 was determined by the crude ¹H NMR spectra of the reaction mixture.

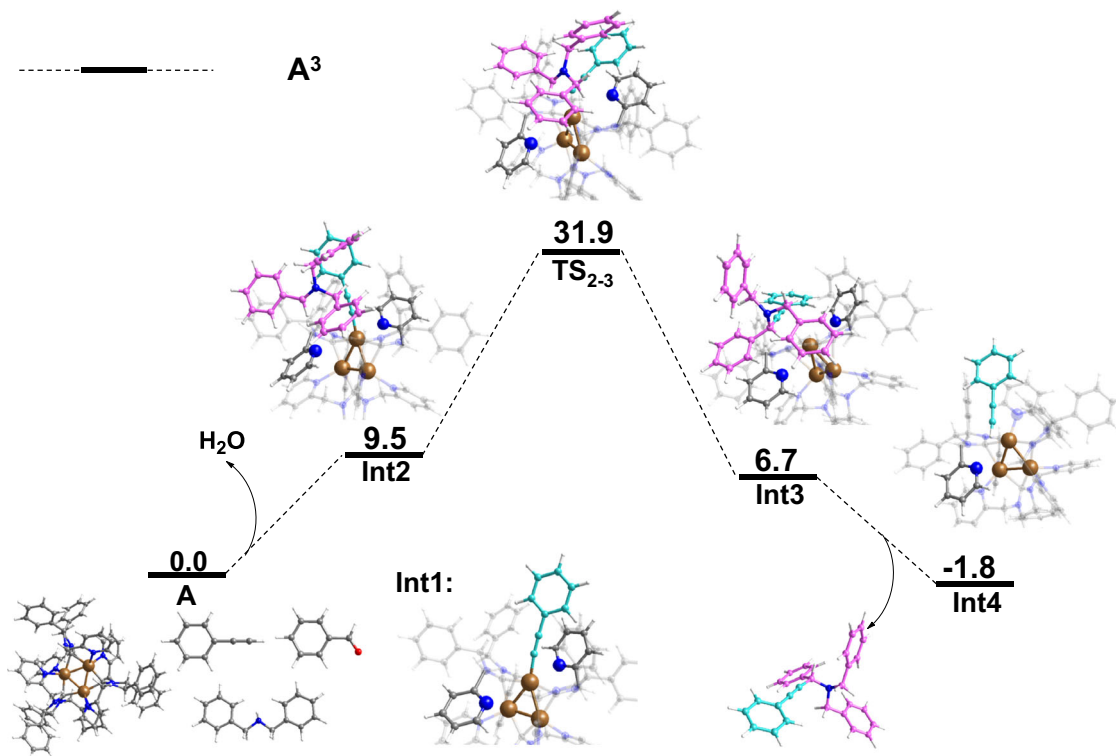


Fig. 5 | Theoretical calculations. DFT-computed Gibbs free energy profile (ΔG in kcal/mol) for the formation of the propargylamine.

To clarify the catalytic mechanism of the A³ coupling reaction, DFT calculations were performed on the specific compounds applied experimentally: benzaldehyde (1), phenylacetylene (2) and dibenzylamine (3) with the Cu₃NC^(NHC) catalyst (Fig. 5). The A³ coupling reaction commences when one pyridine of N-heterocyclic carbene could

dynamically dissociate from the copper atom of Cu₃NC^(NHC) in the organic transformation, exposing the catalytic copper sites of the Cu₃NC^(NHC) and activating the phenylacetylene (2) substrate. Then the other pyridine of the N-heterocyclic carbene dynamically dissociates from the single copper atom of Cu₃NC^(NHC) to release more

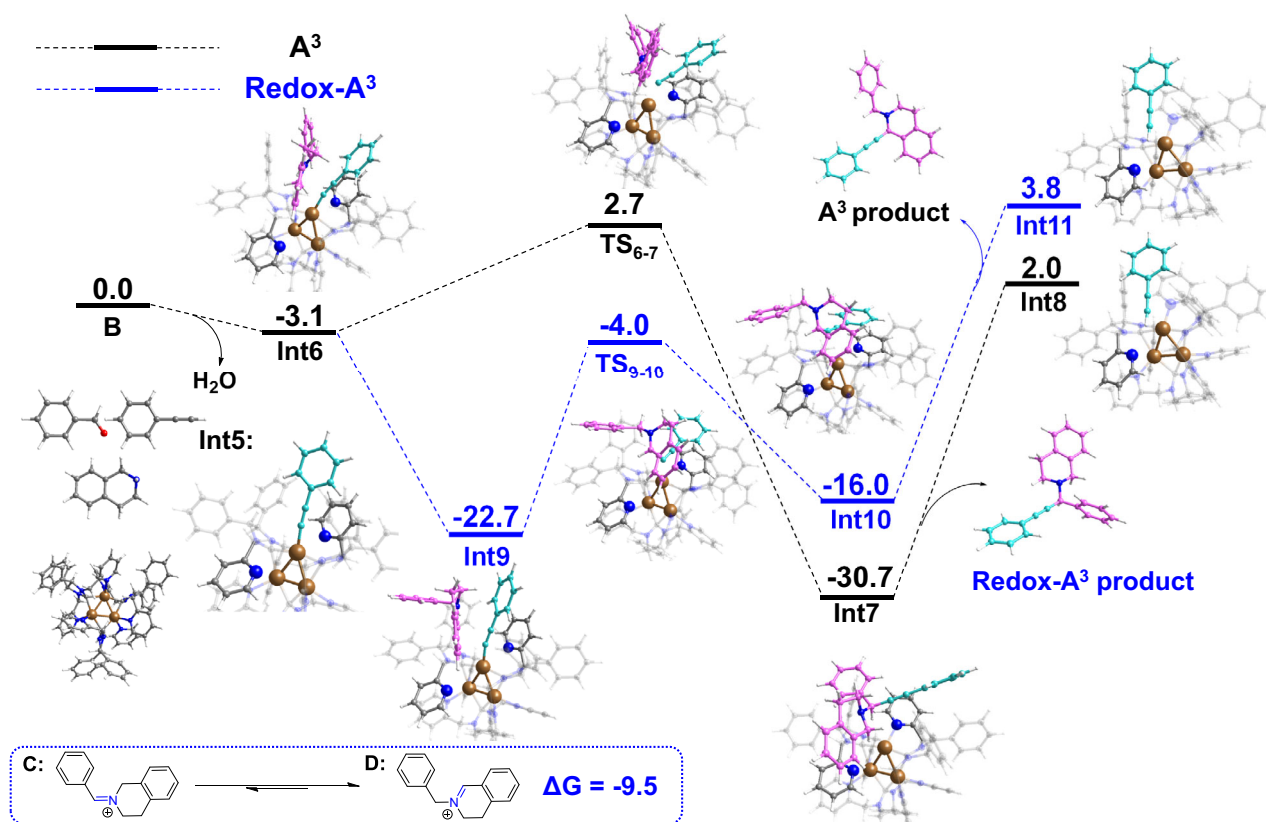


Fig. 6 | Theoretical calculations. DFT-computed Gibbs free energy profile (ΔG in kcal/mol) for the formation of the C1-propargylamines.

space and in situ generate copper acetylide under weak bases environment. Notably, the C–Cu bonds between the NHC ligands and Cu₃ core have always been very stable during the organic transformation process to keep catalyst integrity. The in situ-generated copper acetylide Int1 and iminium cation B afford the ion pair Int2. This process from initial state A to ion pair Int2 leads to an energy increase of 9.5 kcal/mol and produces one molecule of water. Subsequently, the reaction of copper acetylide Int1 and iminium cation B could form propargylamine–Cu₃NC^(NHC) complex Int3 via the transition state TS_{2,3}, which requires an energy barrier of 31.9 kcal/mol. Next one molecule of propargylamine is dissociated from complex Int3. Furthermore, the half of dissociated Cu–N bond is reformed, and another molecule of phenylacetylene (2) is activated by the Cu₃NC^(NHC) catalyst with exposed active catalytic sites to obtain the catalyst Int4, which could enter the next cycle.

To gain a deep understanding of the origin of the highly reactive and regioselective redox-A³ coupling reaction, we performed the DFT calculations with THIQs as the amine substrate replacing dibenzylamine in this system (Fig. 6). The condensation of benzaldehyde (1) with THIQs produces *exo*-iminium ion D, and this process of forming the ion pair Int6 leads to an energy decrease of 3.1 kcal/mol and produces one molecule of water. The *exo*-iminium ion D is very easy to convert to a more stable *endo*-iminium ion E through releasing energy of 9.5 kcal/mol. It is very beneficial that the ion pair Int6 converts to a more stable ion pair Int9 by releasing energy of 19.6 kcal/mol. It means that the intermediate ion pair Int9 is a more stable and easier to produce than ion pair Int6. In addition, according to the energetic span model^{59,60}, the overall barrier of the A³ coupling reaction is 33.4 kcal/mol, corresponding to the energy difference between the first Int7 and the second TS₆₋₇, requiring a higher energy barrier than the overall barrier for the redox-A³ coupling reaction (Supplementary Figs. 36 and 37). All these DFT calculation results are greatly helpful to understand the specificity of the Cu₃NC^(NHC) catalyst in the redox-A³ coupling reaction.

Therefore, Cu₃NC^(NHC) as the catalyst could catalyze the redox-A³ coupling reaction with high efficiency and high regioselectivity under mild conditions when the THIQs were used as the amine substrates.

Based on the abovementioned results of control experiments and DFT calculations, the plausible mechanisms for the formation of propargylamines and C1-propargylamines are shown in Fig. 7, which both commence with one pyridine of DLL dynamically dissociating from the Cu₃NC^(NHC) (I) to expose copper catalytic sites, activate the alkyne substrate and afford the intermediate π -metal–alkyne complex (II). The intermediate complex (II) could make the alkyne proton more acidic, which is conducive to the deprotonation of terminal alkyne by the presence of weak bases (amine reactants, *exo*-iminium ions and so on) in the reaction media. The reactions of aldehyde and amine generate in situ *exo*-iminium ions, which then react with the intermediate π -metal–alkyne complex (II). Moreover, the other pyridine of DLL dynamically dissociates from the single copper atom of Cu₃NC^(NHC) to release a relatively high amount of space, which is more conducive to in situ generating the copper acetylides and by-product H₂O under weak bases environment. The by-product H₂O could be removed by the activated MS 4 Å sieves. Then the reaction of in situ-generated copper acetylides and *exo*-iminium ions (via oxidative addition/reductive elimination) could form propargylamines (the A³ coupling product) (Fig. 7, Path A). When in situ-generated *exo*-iminium ions isomerize to *endo*-iminium ions, the *endo*-iminium ions react with the activated intermediate π -metal–alkyne complex (II) to afford the copper acetylides and by-product H₂O. The adsorption drying agent of MS 4 Å sieves could remove by-product water in time, enhancing reactions rate. Next, the metal acetylides react with *endo*-iminium ions, forming C1-propargylamines (the redox-A³ coupling product) through oxidative addition/reductive elimination (Fig. 7, Path B). The dissociated Cu–N bonds of Cu₃NC^(NHC) are reformed, indicating the concomitant regeneration of Cu₃NC^(NHC) (I) in the dehydrogenative coupling transformations; Cu₃NC^(NHC) could enter the next cycle.

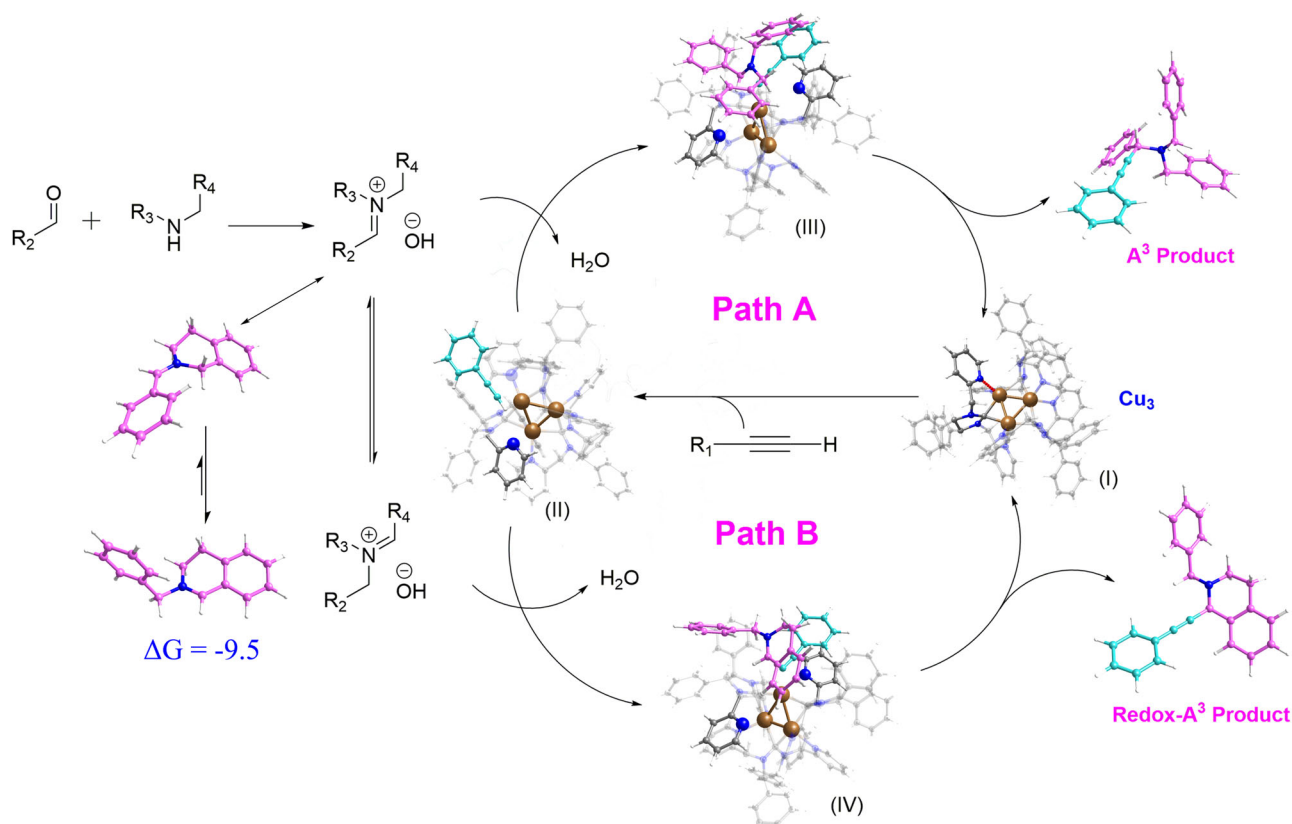


Fig. 7 | Proposed reaction mechanism (ΔG in kcal/mol). Path A catalytic mechanism for the formation of the propargylamines. Path B catalytic mechanism for the formation of the Cl-propargylamines.

To further explore the practical properties of the $\text{Cu}_3\text{NC}^{(\text{NHC})}$ catalyst, preliminary kinetic studies of the A^3 coupling reaction and redox- A^3 coupling reaction were conducted. Both the reactions followed the pseudo-first-order rate dependence on the concentration of phenylacetylenes, as demonstrated by the linear fitting of the $\ln(C_0/C)$ vs. reaction time (t) curve (Supplementary Figs. 38–41). Moreover, both large-scale preparations (2.0 mmol) of propargylamines and Cl-propargylamines were further studied, affording 95% yield of **4a** and 96% yield of **5a** under mild conditions, respectively (Fig. 8a, b). More importantly, the catalytic system of $\text{Cu}_3\text{NC}^{(\text{NHC})}$ could be used for the synthesis of bioactive molecules, such as *N*-ethyl-3-carbazolecarboxaldehyde, to provide propargylamine product **4br** in 90% yield under mild conditions (Fig. 8c). Surprisingly, the diastereoselectivity of the $\text{Cu}_3\text{NC}^{(\text{NHC})}$ -catalyzed A^3 coupling reaction was investigated, in which (*R*)-1-phenyl-1,2,3,4-tetrahydroisoquinoline as a model substrate presented propargylamine product **4bs** with excellent diastereoselectivity (15.8:1) (Fig. 8d). Finally, the investigation found that the $\text{Cu}_3\text{NC}^{(\text{NHC})}$ catalyst displayed excellent stability and reusability in both transformation reactions. The A^3 coupling reaction was conducted six times, and the redox- A^3 coupling reaction was conducted three times with the $\text{Cu}_3\text{NC}^{(\text{NHC})}$ catalyst. Nearly quantitative yields were obtained in all transformations (Supplementary Figs. 42 and 43).

Discussion

In summary, we have successfully developed a rigid-flexible-coupled $\text{Cu}_3\text{NC}^{(\text{NHC})}$ nanocluster in the gram scale, supported by the designed NHC ligand. The atomically precise $\text{Cu}_3\text{NC}^{(\text{NHC})}$ is endowed with a dynamically catalytic center and dual attributes of flexibility and rigidity by dynamic dissociation and coordination of DLL. The ultra-small copper clusters with ultrahigh stability have been used to catalyze highly all-in-one three-component dehydrogenative coupling reactions, including excellent regioselectivity (reaching 100%), high

efficiency (TON = 3800 and 1840), high yield (reaching 99%), broad substrate scopes (85 examples) and mild conditions (room temperature). Mechanistic and control experimental studies have demonstrated that the remarkable catalytic properties originate from the rigid and flexible dual attributes of the $\text{Cu}_3\text{NC}^{(\text{NHC})}$ catalyst. The origin of the enhanced regioselectivity catalyzed by $\text{Cu}_3\text{NC}^{(\text{NHC})}$ is associated with the energy of the ion pair with copper acetylide and iminium cation, leading to modulation of the activation barrier to obtain a single product. This work illustrates the precise structure–activity relationship of nanoclusters and provides a reference for using metal nanoclusters in homogenous organic transformations, which can build a bridge between metal nanoclusters catalyst and organic pharmaceutical chemistry and promote more exploration of metal nanocluster-catalyzed organic reactions.

Methods

All the reactions were carried out under ambient atmosphere (air) conditions unless otherwise noted. All commercial reagents and solvents were obtained from the commercial provider and used without further purification. ^1H NMR and ^{13}C NMR spectra were recorded on Bruker 600 MHz spectrometers. Chemical shifts were reported relative to internal tetramethylsilane (δ 0.00 ppm), CD_3CN (δ 1.94 ppm) or CDCl_3 (δ 7.26 ppm) for ^1H NMR and CDCl_3 (δ 77.0 ppm), CD_3CN (δ 118.3 ppm) for ^{13}C NMR. Flash column chromatography was performed on 300–400 mesh silica gel.

Instrumentation

Powder X-ray diffraction (PXRD) patterns of $\text{Cu}_3\text{NC}^{(\text{NHC})}$, $\text{Cu}_3\text{NC}^{(\text{BINAP})}$, and $\text{Cu}_3\text{NC}^{(\text{Pz})}$ were recorded on a Rigaku B/Max-RB X-ray diffractometer with Cu-K α radiation ($\lambda = 1.5418 \text{ \AA}$) in air at room temperature. ESI-MS images of the clusters were recorded on an AB Sciex X500R Q-TOF spectrometer. UV–vis absorption spectra were obtained

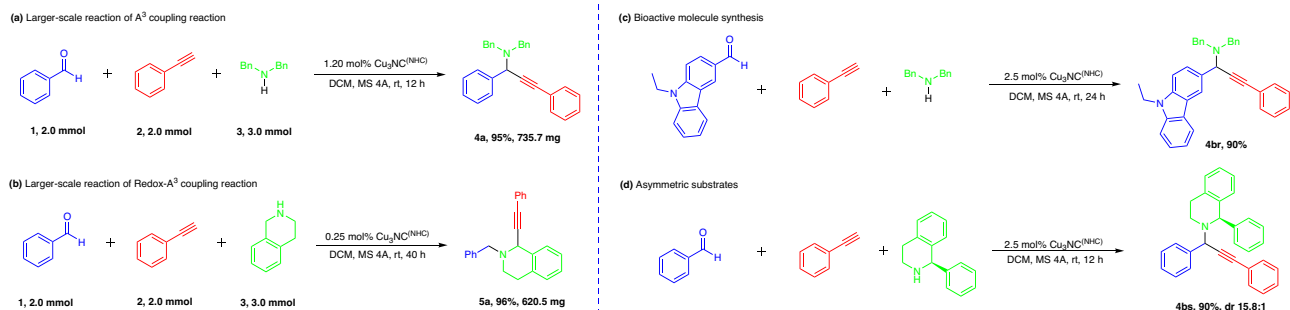


Fig. 8 | The catalytic performance of $\text{Cu}_3\text{NC}^{\text{(NHC)}}$. **a** Large-scale synthesis of the desired propargylamine product **4a**. **b** Large-scale synthesis of the desired C1-propargylamine product **5a**. **c** Bioactive molecule synthesis under mild conditions.

d Exploration of substrate-controlled asymmetric the $\text{Cu}_3\text{NC}^{\text{(NHC)}}$ -catalyzed A^3 coupling transformation.

through a Hitachi UH4150 UV–visible spectrophotometer. The X-ray diffraction data of $\text{Cu}_3\text{NC}^{\text{(NHC)}}$ and $\text{Cu}_3\text{NC}^{\text{(Pz)}}$ were measured on a Rigaku XtaLAB Pro diffractometer (Supplementary Tables 3 and 4).

Materials

Three-component coupling of aldehydes, alkynes, and amines (including the A^3 coupling reaction and the redox- A^3 reaction) via C–H activation was carried out under the atmosphere of dried and purified N_2 using standard Schlenk. Toluene and THF were dried over sodium/benzophenone and distilled under nitrogen prior to use. DCM was dried over calcium hydride and distilled under nitrogen prior to use. Ethanol and methanol were dried over iodine/magnesium strips and distilled under nitrogen prior to use. The other dry solvent including 1,4-dioxane, acetonitrile and DCE were directly purchased from Energy Chemical. BINAP, 3,5-diphenyl-pyrazole, aldehydes, alkynes and amines were purchased from Bidepharm, Energy Chemical and Heowns without further purification. The Vulcan XC-72 carbon black was purchased from Macklin.

Synthesis of 4,5-diphenyl-4,5-dihydro-1H-imidazole⁶¹

Under N_2 atmosphere, 1,2-diphenylethylenediamine (3.0 g, 14.1 mmol), dry MeOH (100.0 mL) and formylformic acid (1.5 g, 16.3 mmol) were added into the dry round-bottom flask in turn. The reaction mixture was stirred at room temperature for 4 h. Then NBS (3.0 g, 18.54 mmol) was added into the stirred mixture of the round-bottom flask and the reaction mixture was stirred at room temperature for 20 h. The reaction was monitored by TLC. When 1,2-diphenylethylenediamine was consumed, the reaction was quenched by adding sat. $\text{Na}_2\text{S}_2\text{O}_5$ (aq.), then concentrated. The residue was added to 5.0% NaOH (aq.) and was extracted by EA. The organic phase was dried by Na_2SO_4 , then concentrated. The crude product was then purified by column chromatography to give the 4,5-diphenyl-4,5-dihydro-1H-imidazole as white solid with overall isolated yield 90%. ^1H NMR (600 MHz, CDCl_3) δ 7.36–7.32 (m, 4H), 7.29 (t, J = 7.3 Hz, 2H), 7.26–7.23 (m, 4H), 4.70 (s, 2H).

Synthesis of 4,5-diphenyl-1,3-bis(pyridin-2-ylmethyl)–4,5-dihydro-1H-imidazol-3-ium chloride⁶²

Under N_2 atmosphere, 4,5-diphenyl-4,5-dihydro-1H-imidazole (1.1 g, 5.0 mmol), NaHCO_3 (1.3 g, 15.0 mmol), dry EtOH (50.0 mL) and 2-(Chloromethyl) pyridine hydrochloride (1.7 g, 10.3 mmol) were added into the dry round-bottom flask in turn. The reaction mixture was stirred and refluxed at 80 °C by oil bath for 2 days. The reaction was monitored by TLC. When 4,5-diphenyl-4,5-dihydro-1H-imidazole was consumed, the reaction was shut down to cool to ambient temperature, then concentrated. The crude product was then purified by column chromatography to give the 4,5-diphenyl-1,3-bis(pyridin-2-ylmethyl)–4,5-dihydro-1H-imidazol-3-ium chloride as white solid with

overall isolated yield 92%. ^1H NMR (600 MHz, CD_3CN) δ 9.44 (s, 1H), 8.69 (d, J = 4.3 Hz, 2H), 7.75 (td, J = 7.7, 1.7 Hz, 2H), 7.45–7.39 (m, 6H), 7.36 (dd, J = 7.1, 5.1 Hz, 2H), 7.29 (dd, J = 7.7, 1.6 Hz, 4H), 7.23 (d, J = 7.7 Hz, 2H), 5.09 (d, J = 16.0 Hz, 2H), 5.02 (s, 2H), 4.39 (d, J = 16.0 Hz, 2H). ^{13}C NMR (151 MHz, CD_3CN) δ 161.5, 153.9, 150.7, 138.4, 136.4, 130.8, 130.4, 129.0, 124.6, 124.0, 74.0, 51.5.

Synthesis of $\text{Cu}_3\text{NC}^{\text{(NHC)}}$

Under N_2 atmosphere, 4,5-diphenyl-1,3-bis(pyridin-2-ylmethyl)–4,5-dihydro-1H-imidazol-3-ium chloride (440.2 mg, 1.0 mmol) was dissolved in 20 mL of H_2O , to which 20 mL of H_2O solution containing KPF_6 (404.8 mg, 2.2 mmol) was added under vigorous stirring at room temperature. The suspension was centrifuged and the white solid was collected. The white solid was dissolved in 30.0 mL of MeCN. Overabundant Cu power (320 mg, 5.0 mmol) was then added to the stirred mixture. The reaction mixture was stirred at room temperature for 24 h. After filtration and concentration, diethyl ether was added to obtain the crude product. The crude product was dissolved in acetonitrile, and the resulting solution was diffused with diethyl ether in vapor phase to obtain colorless crystals of $\text{Cu}_3\text{NC}^{\text{(NHC)}}$ (Yield: 67.8%, calculated based on NHC ligand) for 5 days at room temperature. ^1H NMR (600 MHz, CD_3CN) δ 8.48 (d, J = 4.3 Hz, 6H), 7.99 (t, J = 7.4 Hz, 6H), 7.63–7.56 (m, 6H), 7.51–7.28 (m, 30H), 7.23 (d, J = 7.5 Hz, 6H), 4.93 (s, 6H), 4.17 (d, J = 15.6 Hz, 6H), 3.50 (d, J = 15.7 Hz, 6H). ^{13}C NMR (151 MHz, CD_3CN) δ 154.2, 152.3, 141.2, 132.2, 131.1, 130.4, 126.4, 126.1, 72.0, 53.0.

Synthesis of $\text{Cu}_3\text{NC}^{\text{(BINAP)42}}$

BINAP (0.045 g, 0.07 mmol) and $^t\text{BuScu}$ (0.025 g, 0.16 mmol) were well mixed in 15 mL acetonitrile/toluene (volume ratio 2:1) at room temperature. The mixture was treated under ultrasonic conditions until a clear solution was obtained. Then 250 μLCS_2 was added. The solution quickly turned to tawny when exposed to air. The tawny solution was allowed to evaporate slowly in darkness at room temperature. After ~5 days, yellow block crystals of $\text{Cu}_3\text{NC}^{\text{(BINAP)}}$ were obtained in a yield of 49.0% (calculated based on BINAP). ^1H NMR (400 MHz, DMSO) δ 7.98 (s, 12H), 7.59 (d, J = 8.1 Hz, 12H), 7.44–7.29 (m, 20H), 7.25 (t, J = 7.5 Hz, 5H), 7.15 (dd, J = 15.0, 7.1 Hz, 12H), 6.73 (dd, J = 34.8, 27.5 Hz, 23H), 6.45 (s, 12H), 1.10 (s, 9H).

Synthesis of $\text{Cu}_3\text{NC}^{\text{(Pz)43}}$

$\text{Cu}(\text{CH}_3\text{CN})_4\text{PF}_6$ (358 mg, 0.96 mmol) and 3,5-diphenyl-pyrazole (212 mg, 0.96 mmol) were dissolved in 5 mL acetone. The mixture was stirred to provide a clear, slightly green solution. The NEt_3 (0.16 mL, 1.15 mmol) was added to stirred solution by dropwise and formed a white precipitate, which was stirred for 30 min, then filtered, washed with acetone and vacuum-dried. Finally, the product was dissolved in DCM– Et_2O solution, and colorless crystals of $\text{Cu}_3\text{NC}^{\text{(Pz)}}$ were

obtained in a yield of 80% (218 mg). ^1H NMR (600 MHz, CDCl_3) δ 7.69 (d, $J=7.5$ Hz, 12H), 7.20 (t, $J=7.3$ Hz, 8H), 7.06 (t, $J=7.5$ Hz, 12H), 6.76 (s, 4H). ^{13}C NMR (151 MHz, CDCl_3) δ 155.1, 132.6, 128.6, 128.0, 126.6, 102.2.

General procedure for $\text{Cu}_3\text{NC}^{\text{(NHC)}}$ -catalyzed the A^3 coupling reaction

Under N_2 atmosphere, the catalyst of $\text{Cu}_3\text{NC}^{\text{(NHC)}}$ (2.5 mol%), activated MS 4 Å sieves (600 mg) and dry DCM (1.5 mL) were added into the dry Schlenk tube. The reaction mixture was stirred at room temperature for 5 min. Aldehydes 1 (0.1 mmol or 0.2 mmol) and alkynes 2 (0.2 mmol or 0.1 mmol) were then added to the stirred mixture. The reaction mixture was stirred at room temperature for 5 minutes. Amines 3 (0.3 mmol, 1.5 eq) and dry DCM (0.5 mL, 0.1 M) were added into the stirred mixture of the Schlenk tube. The reactions were stirred at room temperature for 12 h. The reactions were monitored by TLC. When aldehydes 1 and alkynes 2 were consumed, the reactions were quenched and concentrated. The crude products were then purified by column chromatography to give the target molecules.

General procedure for $\text{Cu}_3\text{NC}^{\text{(NHC)}}$ -catalyzed the redox- A^3 coupling reaction

Under N_2 atmosphere, the catalyst of $\text{Cu}_3\text{NC}^{\text{(NHC)}}$ (0.25 mol%), activated MS 4 Å sieves (600 mg) and dry DCM (1.5 mL) were added into the dry Schlenk tube. The reaction mixture was stirred at room temperature for 5 min. Aldehydes 1 (0.2 mmol, 1.0 eq.) and alkynes 2 (0.2 mmol, 1.0 eq.) were then added to the stirred mixture. The reaction mixture was stirred at room temperature for 5 minutes. The 1,2,3,4-tetrahydroisoquinoline 3 (0.3 mmol, 1.5 eq.) and dry DCM (0.5 mL, 0.1 M) were added into the stirred mixture of the Schlenk tube. The reactions were stirred at room temperature for 40 h. The reactions were monitored by TLC. When aldehydes 1 and alkynes 2 were consumed, the reactions were quenched and concentrated. The crude products were then purified by column chromatography to give the target molecules.

General procedure for $\text{Cu}_3\text{NC}^{\text{(NHC)}}$ -catalyzed the A^3 coupling reaction in 2 mmol scale

Under N_2 atmosphere, the catalyst of $\text{Cu}_3\text{NC}^{\text{(NHC)}}$ (46 mg, 1.2 mol%), activated MS 4 Å sieves (5.0 g) and dry DCM (15.0 mL) were added into the dry Schlenk tube. The reaction mixture was stirred at room temperature for 5 min. Benzaldehyde 1 (213 mg, 2.0 mmol, 1.0 eq.) and phenylacetylene 2 (205.0 mg, 2.0 mmol, 1.0 eq.) were then added to the stirred mixture. The reaction mixture was stirred at room temperature for 5 min. Dibenzylamine 3 (592.0 mg, 3.0 mmol, 1.5 eq.) and dry DCM (5.0 mL, 0.1 M) were added into the stirred mixture of the Schlenk tube. The reaction was stirred at room temperature for 12 h. The reactions were monitored by TLC. When Benzaldehyde 1 and Phenylacetylene 2 were consumed, the reaction was quenched and concentrated. The crude product was then purified by column chromatography (PE-EA, v/v 10/1) to give the N, N-dibenzyl-1,3-diphenylprop-2-yn-1-amine (**4a**) as colorless oil with overall isolated yield: 95% (735.7 mg).

General procedure for $\text{Cu}_3\text{NC}^{\text{(NHC)}}$ -catalyzed the redox- A^3 coupling reaction in 2 mmol scale

Under N_2 atmosphere, the catalyst of $\text{Cu}_3\text{NC}^{\text{(NHC)}}$ (9.2 mg, 0.25 mol%), activated MS 4 Å sieves (5.0 g) and dry DCM (15.0 mL) were added into the dry Schlenk tube. The reaction mixture was stirred at room temperature for 5 min. Benzaldehyde 1 (213 mg, 2.0 mmol, 1.0 eq.) and phenylacetylene 2 (205.0 mg, 2.0 mmol, 1.0 eq.) were then added to the stirred mixture. The reaction mixture was stirred at room temperature for 5 min. The 1,2,3,4-Tetrahydroisoquinoline 3 (400.0 mg, 3.0 mmol, 1.5 eq.) and dry DCM (5.0 mL, 0.1 M) were added into the stirred mixture of the Schlenk tube. The reaction was stirred at room temperature for 40 h. The reactions were monitored by TLC. When Benzaldehyde 1 and Phenylacetylene 2 were consumed, the reaction

was quenched and concentrated. The crude product was then purified by column chromatography (PE-EA, v/v 10/1) to give the 2-benzyl-1-(phenylethynyl)-1,2,3,4-tetrahydroisoquinoline (**5a**) as pale-yellow oil with overall isolated yield: 96% (620.5 mg).

Recycling procedure for $\text{Cu}_3\text{NC}^{\text{(NHC)}}$ -catalyzed the A^3 coupling reaction

Under N_2 atmosphere, the catalyst of $\text{Cu}_3\text{NC}^{\text{(NHC)}}$ (2.5 mol%), activated MS 4 Å sieves (600 mg) and dry DCM (1.5 mL) were added into the dry Schlenk tube. The reaction mixture was stirred at room temperature for 5 minutes. Aldehydes 1 (0.2 mmol, 1.0 eq.) and alkynes 2 (0.2 mmol, 1.0 eq.) were then added to the stirred mixture. The reaction mixture was stirred at room temperature for 5 minutes. Amines 3 (0.3 mmol, 1.5 eq.) and dry DCM (0.5 mL, 0.1 M) were added into the stirred mixture of the Schlenk tube. The reaction was stirred at room temperature for 12 h. Conversion and yield were determined by ^1H NMR using 1,3,5-trimethoxybenzene as an internal standard. Then the reactants [aldehydes 1 (0.2 mmol, 1.0 eq.), alkynes 2 (0.2 mmol, 1.0 eq.), and amines 3 (0.3 mmol, 1.5 eq.)] were injected to the reaction system five consecutive times, subsequently. Every conversion and yield were determined by ^1H NMR using 1,3,5-trimethoxybenzene as an internal standard.

Recycling procedure for $\text{Cu}_3\text{NC}^{\text{(NHC)}}$ -catalyzed the redox- A^3 coupling reaction

Under N_2 atmosphere, the catalyst of $\text{Cu}_3\text{NC}^{\text{(NHC)}}$ (0.25 mol%), activated MS 4 Å sieves (600 mg) and dry DCM (1.5 mL) were added into the dry Schlenk tube. The reaction mixture was stirred at room temperature for 5 min. Aldehydes 1 (0.2 mmol, 1.0 eq.) and alkynes 2 (0.2 mmol, 1.0 eq.) were then added to the stirred mixture. The reaction mixture was stirred at room temperature for 5 min. The 1,2,3,4-Tetrahydroisoquinoline 3 (0.3 mmol, 1.5 eq.) and dry DCM (0.5 mL, 0.1 M) were added into the stirred mixture of the Schlenk tube. The reaction was stirred at room temperature for 40 h. Conversion and yield were determined by ^1H NMR using 1,3,5-trimethoxybenzene as an internal standard. Then the reactants [aldehydes 1 (0.2 mmol, 1.0 eq.), alkynes 2 (0.2 mmol, 1.0 eq.) and amines 3 (0.3 mmol, 1.5 eq.)] were injected to the reaction system two consecutive times, subsequently. Every conversion and yield were determined by ^1H NMR using 1,3,5-trimethoxybenzene as an internal standard.

Catalytic mechanism studies by density functional theory (DFT) calculations

DFT calculations were conducted using the Gaussian 16 package, specifically at the B3LYP-D3 level of theory, where dispersion interactions were considered^{63–68}. For carbon, oxygen, hydrogen, and nitrogen atoms, the 6-31G* basis set was employed, while the 6-311++G** basis set was utilized for copper^{69,70}. To account for solvation effects, single-point calculations were performed using the solvation model based on density (SMD) in dichloromethane⁷¹. Vibrational frequency calculations were conducted to verify that a transition state exhibits only one imaginary frequency and a local minimum displays no imaginary frequency. Transition states connecting the relevant minima were further investigated through intrinsic reaction coordinate (IRC) calculations^{72–74}. Corrections of -2.6 (or 2.6) kcal/mol were applied for transformations involving the conversion of two molecules to one (or one molecule to two) to obtain relative Gibbs energies at 298 K. This approach has been used in numerous previous studies to minimize the overestimation of entropy contributions^{75–83}.

According to the energetic span model, the schematic illustration of the energy profile given the A^3 coupling reaction and the redox- A^3 coupling reaction in Fig. 6, including the energy profile for an additional catalytic cycle (THIQs as the amine substrate). TS_{6-7} , TS_{9-10} , Int_7 , and Int_9 represent rate-determining transition states and intermediates, respectively. We could also view the first Int_7 to the second

TS_{6,7} as a catalytic cycle from Supplementary Fig. 36. The first TS_{9,10} to the second Int9 could be viewed as a catalytic cycle from Supplementary Fig. 37. Therefore, the overall barrier of A³ coupling and redox-A³ coupling could be calculated by $\Delta G_1 + \Delta G_2$ and $\Delta G_3 + \Delta G_4$, respectively. We obtained $\Delta G_1 = 27.6 \text{ kcal mol}^{-1}$, $\Delta G_2 = 5.8 \text{ kcal mol}^{-1}$, $\Delta G_3 = 19.8 \text{ kcal mol}^{-1}$ and $\Delta G_4 = 6.7 \text{ kcal mol}^{-1}$ from Fig. 6.

Data availability

All other data are available from the corresponding author upon request. All data needed to evaluate the conclusions in the paper are present in the paper and/or the Supplementary Materials (including Supplementary Figs. 1–226, details of the chemicals, instrumentation, synthesis, characterization, DFT and X-ray crystal details for Cu₃NC^(NH₃) (CIF) and Cu₃NC^(Pz) (CIF)). The source data for Figs. 5 and 6 are provided with this paper. The X-ray crystallographic coordinates for the structures reported in this article have been deposited at the Cambridge Crystallographic Data Centre (CCDC), under deposition number CCDC 2268919 (Cu₃NC^(NH₃)) 2268920 (Cu₃NC^(Pz)). These data can be obtained free of charge via www.ccdc.cam.ac.uk/data_request/cif. Source data are provided with this paper.

References

- Lauder, K., Toscani, A., Scalacci, N. & Castagnolo, D. Synthesis and reactivity of propargylamines in organic chemistry. *Chem. Rev.* **117**, 14091–14200 (2017).
- Peshkov, V. A., Pereshivko, O. P. & Van der Eycken, E. V. A walk around the A³-coupling. *Chem. Soc. Rev.* **41**, 3790–3807 (2012).
- Seidel, D. The redox-A³ reaction. *Org. Chem. Front.* **1**, 426–429 (2014).
- Zhang, Y., Huang, L., Li, X., Wang, L. & Feng, H. Chemo- and diastereoselective synthesis of n-propargyl oxazolines through a copper-catalyzed domino A³ reaction. *J. Org. Chem.* **84**, 5046–5055 (2019).
- Bisai, V., Suneja, A. & Singh, V. K. Asymmetric alkynylation/lactamization cascade: An expeditious entry to enantiomerically enriched isoindolinones. *Angew. Chem. Int. Ed.* **53**, 10737–10741 (2014).
- Singh, P. et al. Pyridine-fused 2-pyridones via povarov and A³ reactions: Rapid generation of highly functionalized tricyclic heterocycles capable of amyloid fibril binding. *J. Org. Chem.* **84**, 3887–3903 (2019).
- Kelleher, C. J., Cardozo, L., Chapple, C. R., Haab, F. & Ridder, A. M. Improved quality of life in patients with overactive bladder symptoms treated with solifenacin. *BJU Int.* **95**, 81–85 (2005).
- Zhang, A., Neumeyer, J. L. & Baldessarini, R. J. Recent progress in development of dopamine receptor subtype-selective agents: potential therapeutics for neurological and psychiatric disorders. *Chem. Rev.* **107**, 274–302 (2017).
- Ye, K. et al. Opium alkaloid noscapine is an antitumor agent that arrests metaphase and induces apoptosis in dividing cells. *Proc. Natl Acad. Sci. USA* **95**, 1601–1606 (1998).
- Aubrecht, K. B., Winemiller, M. D. & Callum, D. B. BF₃-mediated addition of lithium phenylacetylide to an imine: correlations of structures and reactivities. BF₃-R₃N derivatives as substitutes for BF₃·Et₂O. *J. Am. Chem. Soc.* **122**, 11084–11089 (2000).
- Rokade, B. V., Barker, J. & Guiry, P. J. Development of and recent advances in asymmetric A³ coupling. *Chem. Soc. Rev.* **48**, 4766–4790 (2019).
- Mo, J. N., Su, J. Q. & Zhao, J. N. The asymmetric A³(aldehyde-alkyne-amine) coupling: highly enantioselective access to propargylamines. *Molecules* **24**, 1216 (2019).
- Fan, W., Yuan, W. & Ma, S. Unexpected e-stereoselective reductive A³-coupling reaction of terminal alkynes with aldehydes and amines. *Nat. Commun.* **5**, 3884 (2014).
- Zhao, C. & Seidel, D. Enantioselective A³ reactions of secondary amines with a Cu(I)/acid-thiourea catalyst combination. *J. Am. Chem. Soc.* **137**, 4650–4653 (2015).
- Paioti, P. H., Abboud, K. A. & Aponick, A. Catalytic enantioselective synthesis of amino skipped diynes. *J. Am. Chem. Soc.* **138**, 2150–2153 (2016).
- Liu, Q. et al. Pyridine ligands for enantioselective syntheses of amines. *Nat. Commun.* **12**, 19 (2021).
- Li, P. & W, L. Mercurous chloride catalyzed mannich condensation of terminal alkynes with secondary amines and aldehydes. *Chin. J. Chem.* **23**, 1076–1080 (2005).
- Sakaguchi, S., Kubo, T. & Ishii, Y. A three-component coupling reaction of aldehydes, amines, and alkynes. *Angew. Chem. Int. Ed.* **40**, 2534–2536 (2001).
- Samai, S., Nandi, G. C. & Singh, M. S. An efficient and facile one-pot synthesis of propargylamines by three-component coupling of aldehydes, amines, and alkynes via C–H activation catalyzed by NiCl₂. *Tetrahedron Lett.* **51**, 5555–5558 (2010).
- Bi, H. P., Zhao, L., Liang, Y. M. & Li, C. J. The copper-catalyzed decarboxylative coupling of the sp³-hybridized carbon atoms of alpha-amino acids. *Angew. Chem. Int. Ed.* **48**, 792–795 (2009).
- Zhang, C. & Seidel, D. Nontraditional reactions of azomethine ylides: decarboxylative three-component couplings of alpha-amino acids. *J. Am. Chem. Soc.* **132**, 1798–1799 (2010).
- Feng, H., Ermolat'ev, D. S., Song, G. & Van der Eycken, E. V. Regioselective Cu(I)-catalyzed tandem A³-coupling/decarboxylative coupling to 3-amino-1,4-enynes. *Org. Lett.* **14**, 1942–1945 (2012).
- Das, D., Sun, A. X. & Seidel, D. Redox-neutral copper(II) carboxylate catalyzed alpha-alkynylation of amines. *Angew. Chem. Int. Ed.* **52**, 3765–3769 (2013).
- Zheng, Q., Meng, W., Jiang, G. & Yu, Z. CuI-catalyzed C1-alkynylation of tetrahydroisoquinolines (THIQs) by A³ reaction with tunable iminium ions. *Org. Lett.* **15**, 5928–5931 (2013).
- Lin, W. et al. Enantioselective double manipulation of tetrahydroisoquinolines with terminal alkynes and aldehydes under copper(I). *Catal. Angew. Chem. Int. Ed.* **53**, 277–281 (2014).
- Zhang, C., Tang, C. & Jiao, N. Recent advances in copper-catalyzed dehydrogenative functionalization via a single electron transfer (SET) process. *Chem. Soc. Rev.* **41**, 3464–3484 (2012).
- Boess, E., Schmitz, C. & Klusmann, M. A comparative mechanistic study of Cu-catalyzed oxidative coupling reactions with n-phenyltetrahydroisoquinoline. *J. Am. Chem. Soc.* **134**, 5317–5325 (2012).
- Liu, L. & Corma, A. Metal catalysts for heterogeneous catalysis: From single atoms to nanoclusters and nanoparticles. *Chem. Rev.* **118**, 4981–5079 (2018).
- Gellé, A. et al. Applications of plasmon-enhanced nanocatalysis to organic transformations. *Chem. Rev.* **120**, 986–1041 (2020).
- Liu, C. Y. et al. Structural transformation and catalytic hydrogenation activity of amidinate-protected copper hydride clusters. *Nat. Commun.* **13**, 2082 (2022).
- Zhao, W. et al. Fe-O clusters anchored on nodes of metal-organic frameworks for direct methane oxidation. *Angew. Chem. Int. Ed.* **60**, 5811–5815 (2021).
- Jin, R., Zeng, C., Zhou, M. & Chen, Y. Atomically precise colloidal metal nanoclusters and nanoparticles: fundamentals and opportunities. *Chem. Rev.* **116**, 10346–10413 (2016).
- Du, Y., Sheng, H., Astruc, D. & Zhu, M. Atomically precise noble metal nanoclusters as efficient catalysts: a bridge between structure and properties. *Chem. Rev.* **120**, 526–622 (2019).
- Jin, R., Li, G., Sharma, S., Li, Y. & Du, X. Toward active-site tailoring in heterogeneous catalysis by atomically precise metal nanoclusters with crystallographic structures. *Chem. Rev.* **121**, 567–648 (2021).

35. Herzing, A. A., Kiely, C. J., Carley, A. F., Landon, P. & Hutchings, C. J. Identification of active gold nanoclusters on iron oxide supports for CO oxidation. *Science* **321**, 1331–1335 (2008).
36. Shen, H. et al. Highly robust but surface-active: an N-heterocyclic carbene-stabilized Au₂₅ nanocluster. *Angew. Chem. Int. Ed.* **58**, 17731–17735 (2019).
37. Shen, H. et al. N-heterocyclic carbene-stabilized gold nanoclusters with organometallic motifs for promoting catalysis. *J. Am. Chem. Soc.* **144**, 10844–10853 (2022).
38. Shen, H. et al. Surface Coordination of multiple ligands endows N-heterocyclic carbene-stabilized gold nanoclusters with high robustness and surface reactivity. *Angew. Chem. Int. Ed.* **60**, 3752–3758 (2021).
39. Koy, M., Bellotti, P., Das, M. & Glorius, F. N-heterocyclic carbenes as tunable ligands for catalytic metal surfaces. *Nat. Catal.* **4**, 352–363 (2021).
40. Cao, Y. et al. Control of single-ligand chemistry on thiolated Au₂₅ nanoclusters. *Nat. Commun.* **11**, 5498 (2020).
41. Guan, Z. J., Li, J. J., Hu, F. & Wang, Q. M. Structural engineering toward gold nanocluster catalysis. *Angew. Chem. Int. Ed.* **61**, e202209725 (2022).
42. Kong, Y. J. et al. Photoresponsive propeller-like chiral AIE copper(I) clusters. *Angew. Chem. Int. Ed.* **59**, 5336–5340 (2020).
43. Raptis, R. G. & Fackler, J. P. Structure of tris(μ -3,5-diphenylpyrazolato-N,N') tricopper(I). Structural comparisons with the silver(I) and gold(I) pyrazolate trimers. *Inorg. Chem.* **27**, 4179–4182 (1988).
44. Chui, S. S. Y., Ng, M. F. Y. & Che, C.-M. Structure determination of homoleptic AuI, AgI, and CuI aryl/alkylethynyl coordination polymers by X-ray powder diffraction. *Chem. Eur. J.* **11**, 1739–1749 (2005).
45. Slater, J. C. Atomic radii in crystals. *J. Chem. Phys.* **41**, 3199–3204 (1964).
46. Zhang, X. & Corma, A. Supported gold(III) catalysts for highly efficient three-component coupling reactions. *Angew. Chem. Int. Ed.* **47**, 4358–4361 (2008).
47. Datta, K. K. R., Subba Reddy, B. V., Ariga, K. & Vinu, A. Gold nanoparticles embedded in a mesoporous carbon nitride stabilizer for highly efficient three-component coupling reaction. *Angew. Chem. Int. Ed.* **49**, 5961–5965 (2010).
48. Karimi, B., Gholinejad, M. & Khorasani, M. Highly efficient three-component coupling reaction catalyzed by gold nanoparticles supported on periodic mesoporous organosilica with ionic liquid framework. *Chem. Commun.* **48**, 8961–8963 (2012).
49. Li, Q., Das, A., Wang, S., Chen, Y. & Jin, R. Highly efficient three-component coupling reaction catalyzed by atomically precise ligand-protected Au₃₈(SC₂H₄Ph)₂₄ nanoclusters. *Chem. Commun.* **52**, 14298–14301 (2016).
50. Kang, X., Abroshan, H., Wang, S. & Zhu, M. Free valence electron centralization strategy for preparing ultrastable nanoclusters and their catalytic application. *Inorg. Chem.* **58**, 11000–11009 (2019).
51. Qin, Z. et al. A homoleptic alkynyl-ligated [Au₁₃Ag₁₆L₂₄]³⁻ cluster as a catalytically active eight-electron superatom. *Angew. Chem. Int. Ed.* **60**, 970–975 (2021).
52. Wang, Y. M. et al. An atomically precise pyrazolate-protected copper nanocluster exhibiting exceptional stability and catalytic activity. *Angew. Chem. Int. Ed.* **62**, e202218369 (2023).
53. Fan, J. Q., Yang, Y., Tao, C. B. & Li, M. B. Cadmium-doped and pincer ligand-modified gold nanocluster for catalytic KA² reaction. *Angew. Chem. Int. Ed.* **62**, e202215741 (2023).
54. Tang, L., Duan, T., Pei, Y. & Wang, S. Synchronous metal rearrangement on two-dimensional equatorial surfaces of Au–Cu alloy nanoclusters. *ACS Nano* **17**, 4279–4286 (2023).
55. Liu, L., Zhang, X., Gao, J. & Xu, C. Engineering metal–organic frameworks immobilize gold catalysts for highly efficient one-pot synthesis of propargylamines. *Green. Chem.* **14**, 1710–1720 (2012).
56. Khan, R. I. & Pitchumani, K. Quinolinium modified β -cyclodextrin: an ionic ligand towards sustainable A³-coupling and tandem cyclization reactions of aldehydes, amines and alkynes. *Mol. Catal.* **519**, 112151 (2022).
57. Bariwal, J. B., Ermolat, D. S. & Van der Eycken, E. V. Efficient microwave-assisted synthesis of secondary alkylpropargylamines by using A³-coupling with primary aliphatic amines. *Chem. Eur. J.* **16**, 3281–3284 (2010).
58. Giles, R. L., Sullivan, J. D., Steiner, A. M. & Looper, R. E. Addition–hydroamination reactions of propargyl cyanamides: rapid access to highly substituted 2-aminoimidazoles. *Angew. Chem. Int. Ed.* **48**, 3116–3120 (2009).
59. Kozuch, S. & Shaik, S. How to conceptualize catalytic cycles? the energetic span model. *Acc. Chem. Res.* **44**, 101–110 (2011).
60. Li, Y. & Lin, Z. Understanding the reaction mechanisms of Pd-catalyzed oxidation of alcohols and domino oxidation–arylation reactions using phenyl chloride as an oxidant. *Org. Chem. Front.* **1**, 1188–1196 (2014).
61. Murai, K., Morishita, M., Nakatani, R., Fujioka, H. & Kita, Y. Oxidative decarboxylative synthesis of 2-H-imidazolines from glyoxylic acid and 1,2-diamines. *Chem. Commun.* **2008**, 4498–4500 (2008).
62. Magill, A. M. et al. Palladium(II) complexes containing mono-, bi- and tridentate carbene ligands. synthesis, characterisation and application as catalysts in C–C coupling reactions. *J. Organomet. Chem.* **617–618**, 546–560 (2001).
63. Stephens, P. J., Devlin, F. J., Chabalowski, C. F. & Frisch, M. J. Ab initio calculation of vibrational absorption and circular dichroism spectra using density functional force fields. *J. Phys. Chem.* **98**, 11623–11627 (1994).
64. Becke, A. D. Density-functional thermochemistry. III. The role of exact exchange. *J. Chem. Phys.* **98**, 5648–5652 (1993).
65. Lee, C., Yang, W. & Parr, R. G. Development of the colle-salvetti correlation-energy formula into a functional of the electron density. *Phys. Rev. B* **37**, 785–789 (1988).
66. Miehlich, B., Savin, A., Stoll, H. & Preuss, H. Results obtained with the correlation energy density functionals of Becke and Lee, Yang and Parr. *Chem. Phys. Lett.* **157**, 200–206 (1989).
67. Grimme, S. Semiempirical GGA-type density functional constructed with a long-range dispersion correction. *J. Comput. Chem.* **27**, 1787–1799 (2006).
68. Grimme, S. Semiempirical hybrid density functional with perturbative second-order correlation. *J. Chem. Phys.* **124**, 034108 (2006).
69. Hariharan, P. C. & Pople, J. A. The influence of polarization functions on molecular orbital hydrogenation energies. *Theor. Chim. Acta* **28**, 213–222 (1973).
70. Hehre, W. J., Ditchfield, R. & Pople, J. A. Self-consistent molecular orbital methods. XII. Further extensions of gaussian-type basis sets for use in molecular orbital studies of organic molecules. *J. Chem. Phys.* **56**, 2257–2261 (1972).
71. Marenich, A. V., Cramer, C. J. & Truhlar, D. G. Universal solvation model based on solute electron density and on a continuum model of the solvent defined by the bulk dielectric constant and atomic surface tensions. *J. Phys. Chem. B* **113**, 6378–6396 (2009).
72. Fukui, K. Formulation of the reaction coordinate. *J. Phys. Chem.* **74**, 4161–4163 (1970).
73. Maeda, S., Harabuchi, Y., Ono, Y., Taketsugu, T. & Morokuma, K. Intrinsic reaction coordinate: calculation, bifurcation, and automated search. *Int. J. Quantum Chem.* **115**, 258–269 (2015).
74. Fukui, K. The path of chemical reactions - the IRC approach. *Acc. Chem. Res.* **14**, 363–368 (1981).
75. Wang, M., Fan, T. & Lin, Z. DFT Studies on copper-catalyzed arylation of aromatic C–H bonds. *Organometallics* **31**, 560–569 (2012).

76. Fan, T., Sheong, F. K. & Lin, Z. DFT studies on copper-catalyzed hydrocarboxylation of alkynes using CO₂ and hydrosilanes. *Organometallics* **32**, 5224–5230 (2013).
77. Ariafard, A., Brookes, N. J., Stanger, R. & Yates, B. F. DFT study on the mechanism of the activation and cleavage of CO₂ by (NHC)CuEPH₃ (E = Si, Ge, Sn). *Organometallics* **30**, 1340–1349 (2011).
78. Rabitz, H. The foundations for chemical kinetics (Yeremin, E. N.). *J. Chem. Educ.* **59**, A106 (1982).
79. Schoenebeck, F. & Houk, K. N. Ligand-controlled regioselectivity in palladium-catalyzed cross coupling reactions. *J. Am. Chem. Soc.* **132**, 2496–2497 (2010).
80. Yu, H., Lu, Q., Dang, Z. & Fu, Y. Mechanistic study of the rhodium-catalyzed [3+2+2] carbocyclization of alkenylidene cyclopropanes with alkynes. *Chem. Asian J.* **8**, 2262–2273 (2013).
81. Ardura, D., López, R. & Sordo, T. L. Relative gibbs energies in solution through continuum models: effect of the loss of translational degrees of freedom in bimolecular reactions on gibbs energy barriers. *J. Phys. Chem. B* **109**, 23618–23623 (2005).
82. Liu, Q. et al. Revealing a second transmetalation step in the Negishi coupling and its competition with reductive elimination: improvement in the interpretation of the mechanism of biaryl syntheses. *J. Am. Chem. Soc.* **131**, 10201–10210 (2009).
83. Ariafard, A., Ghohe, N. M., Abbasi, K. K., Canty, A. J. & Yates, B. F. Theoretical investigation into the mechanism of 3'-dGMP oxidation by [Pt^{IV}Cl₄](dach). *Inorg. Chem.* **52**, 707–717 (2013).

Acknowledgements

This work was supported by the National Natural Science Foundation of China (No. 21825106, S.-Q.Z.; 92061201, S.-Q.Z.), the China Postdoctoral Science Foundation (2022M722864, T.J.), Zhongyuan Thousand Talents (Zhongyuan Scholars) Program of Henan Province (234000510007, S.-Q.Z.), the Excellent Youth Foundation of Henan Scientific Committee (232300421022, X.-Y.D.) and Zhengzhou University.

Author contributions

S.-Q.Z. and T.J. conceived and designed the idea. T.J. prepared nanocluster catalysts and conducted the organic transformation experiments. Y.-X.L., X.-H.M., and J.A. assisted with the experiments and characterizations. T.J. and X.-Y.D. wrote the manuscript. M.-M.Z. helped with the manuscript revising and data analysis. S.-Q.Z., T.J., and X.-Y.D.

discussed the results and prepared the manuscript. All the authors reviewed and contributed to this paper.

Competing interests

The authors declare no competing interests.

Additional information

Supplementary information The online version contains supplementary material available at <https://doi.org/10.1038/s41467-023-42688-3>.

Correspondence and requests for materials should be addressed to Shuang-Quan Zang.

Peer review information *Nature Communications* thanks the anonymous reviewers for their contribution to the peer review of this work. A peer review file is available.

Reprints and permissions information is available at <http://www.nature.com/reprints>

Publisher's note Springer Nature remains neutral with regard to jurisdictional claims in published maps and institutional affiliations.

Open Access This article is licensed under a Creative Commons Attribution 4.0 International License, which permits use, sharing, adaptation, distribution and reproduction in any medium or format, as long as you give appropriate credit to the original author(s) and the source, provide a link to the Creative Commons licence, and indicate if changes were made. The images or other third party material in this article are included in the article's Creative Commons licence, unless indicated otherwise in a credit line to the material. If material is not included in the article's Creative Commons licence and your intended use is not permitted by statutory regulation or exceeds the permitted use, you will need to obtain permission directly from the copyright holder. To view a copy of this licence, visit <http://creativecommons.org/licenses/by/4.0/>.

© The Author(s) 2023